Supplementary Information

Vibrational analysis of auranofin complexes with cysteine and selenocysteine unveils distinct binding motifs and specific unimolecular reactivity

Roberto Paciotti[a,+,*], Davide Corinti[b,+**], Cecilia Coletti[a], Nazzareno Re[a], Giel Berden[c], Jos Oomens[c], Simonetta Fornarini[b], Maria Elisa Crestoni[b]

[a] Dipartimento di Farmacia, Università G. D'Annunzio Chieti-Pescara, Via dei Vestini 31, Chieti I-66100, Italy

[b] Dipartimento di Chimica e Tecnologie del Farmaco, Università di Roma "La Sapienza", I-00185 Roma, Italy

[c] Radboud University, Institute for Molecules and Materials, FELIX Laboratory, Toernooiveld 7, 6525ED Nijmegen, the Netherlands

*r.paciotti@unich.it ; **davide.corinti@uniroma1.it

[+]The authors contributed equally.

Table of contents

Figure S1: ESI mass spectrum in positive ion mode of the auranofin/cysteine solution.
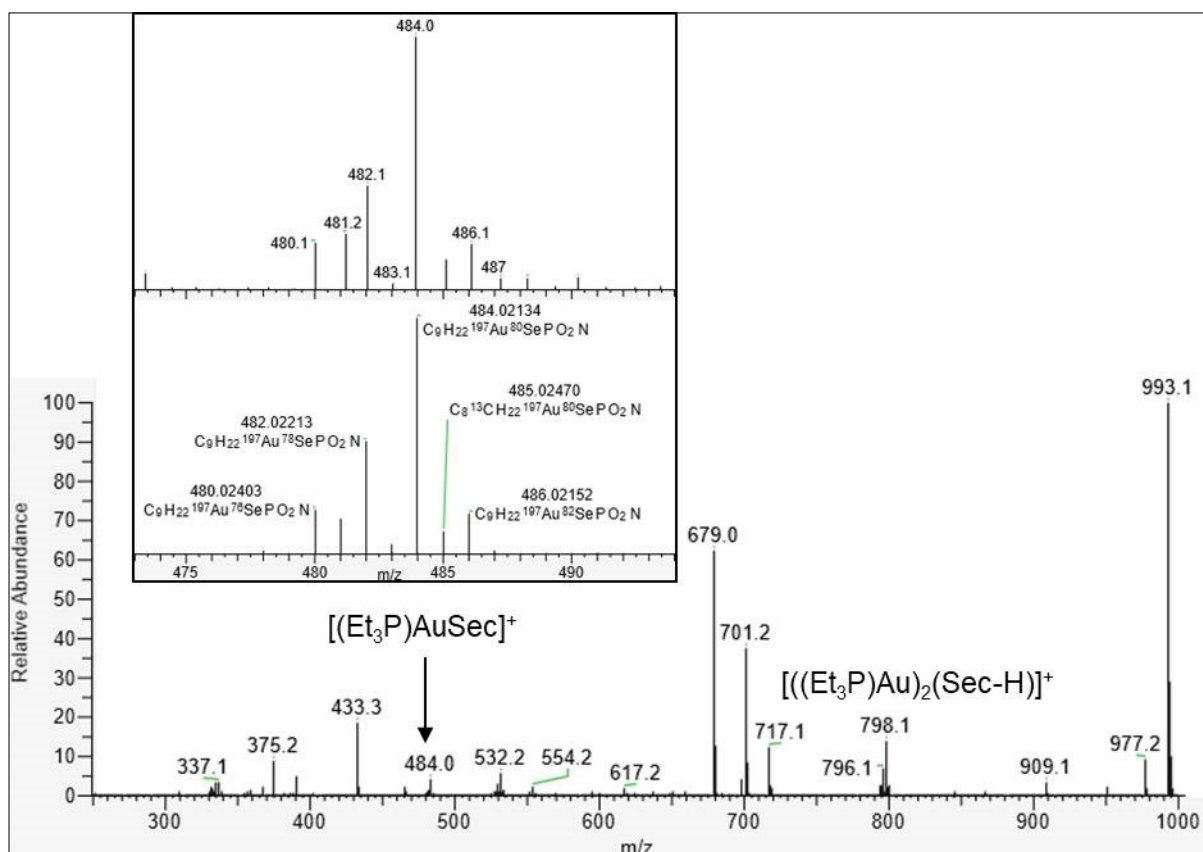
Figure S2: ESI mass spectrum in positive ion mode of the auranofin/selenocysteine solution. The inset shows an enlargement of the [(Et₃P)AuSec]⁺ isotopic cluster (on top) compared to the theoretical one.
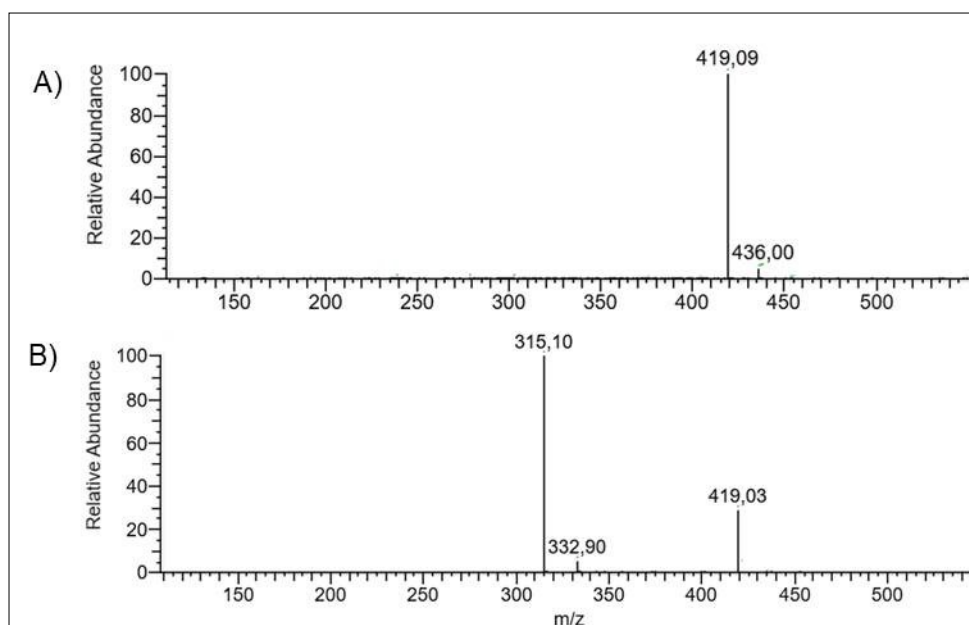
Figure S3: CID mass spectra of A) [(Et₃P)AuCys]⁺ at *m/z* 436 and B) [(Et₃P)Au(Cys-NH₃)]⁺ mass-selected from the CID of *m/z* 436.
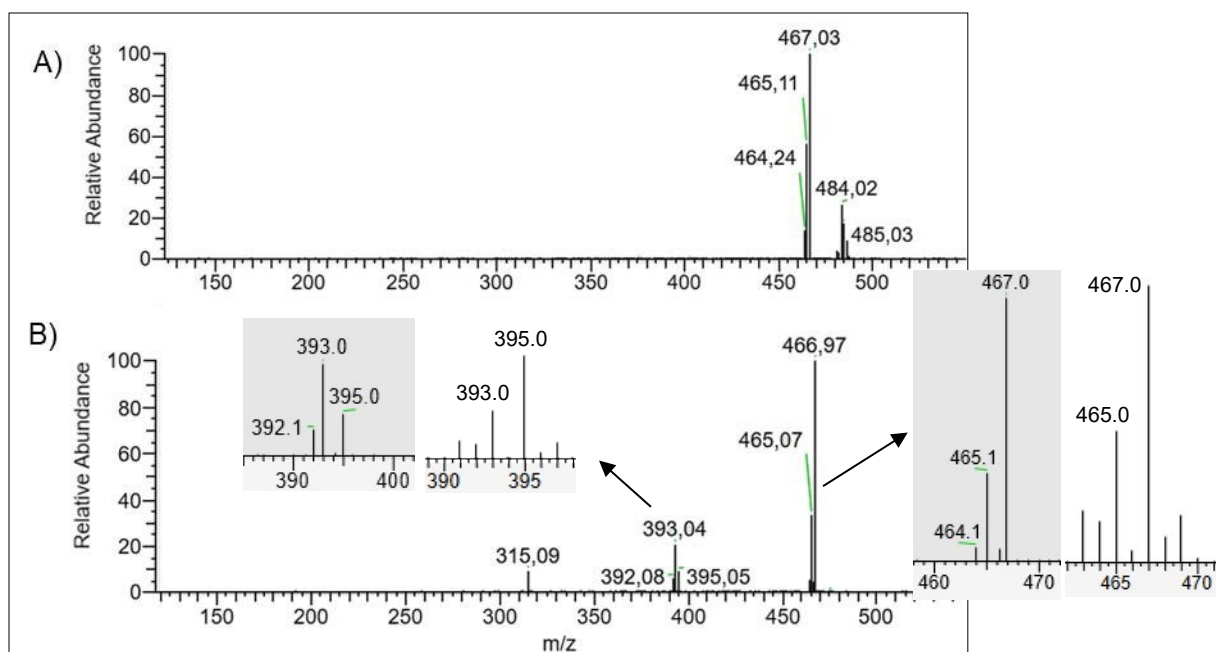
Figure S4: CID mass spectra of A) [(Et₃P)AuSec]⁺ centered at *m/z* 484 and B) [(Et₃P)Au(Sec-NH₃)]⁺ mass-selected from the CID of *m/z* 484. Enlargements of the isotopic clusters of *m/z* 465-467 and *m/z* 393-395 are reported in the insets (left panel, grey background) compared to the calculated ones. Variations in the relative ion abundances are due to the narrow fragmentation window of the instrument, which limits uniform activation of the ions contributing to the isotopic pattern.
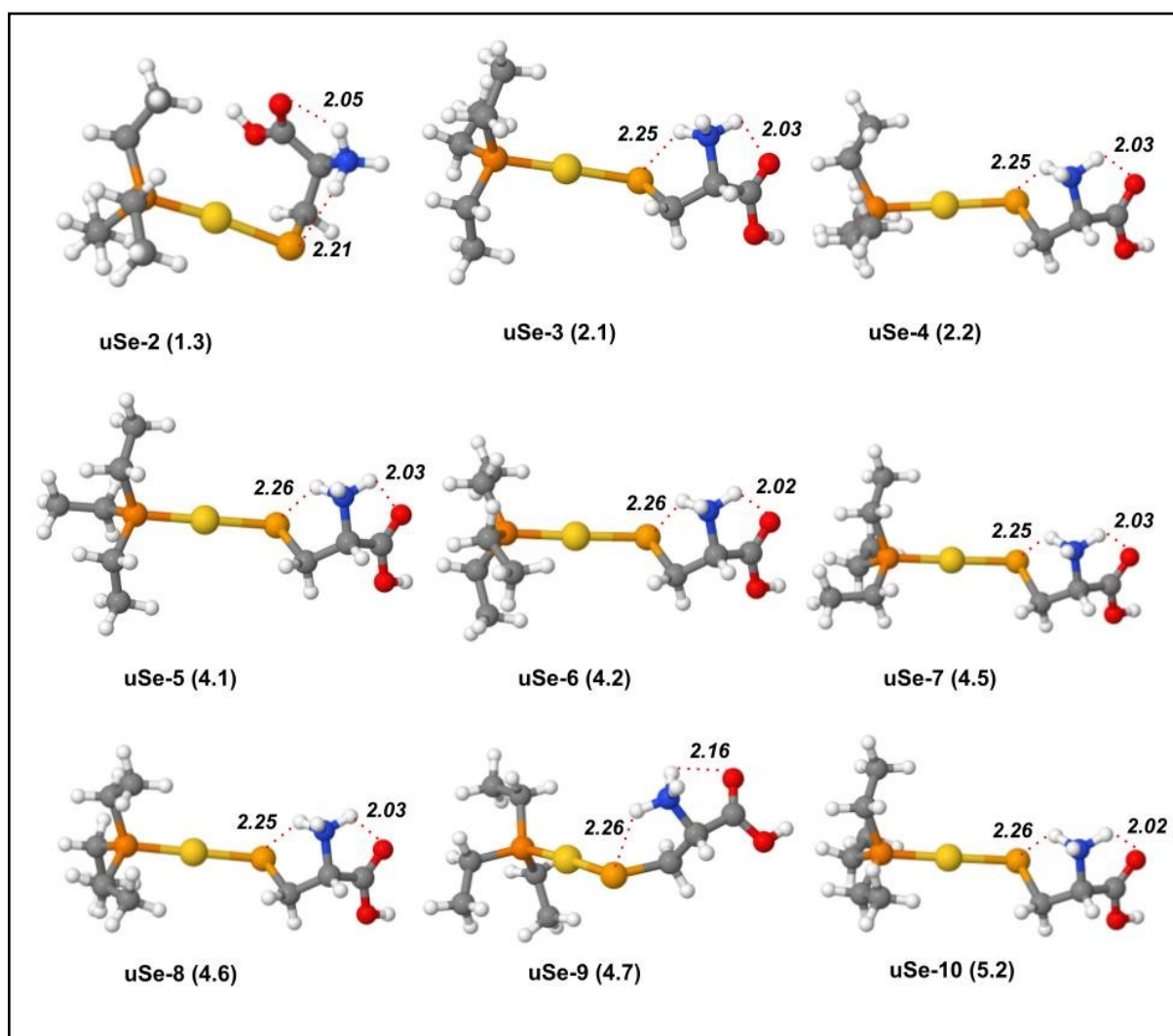
Figure S5: Optimized geometries of the most stable **uSe** conformers of the [(Et$_3$P)AuSec]$^+$ ion, computed in gas phase at B3LYP/BS1 level of theory. Free energy values relative to **uSe-1** are reported in parenthesis in kJ mol^{-1}. Hydrogen bond distances (Å) are indicated by red dotted lines.
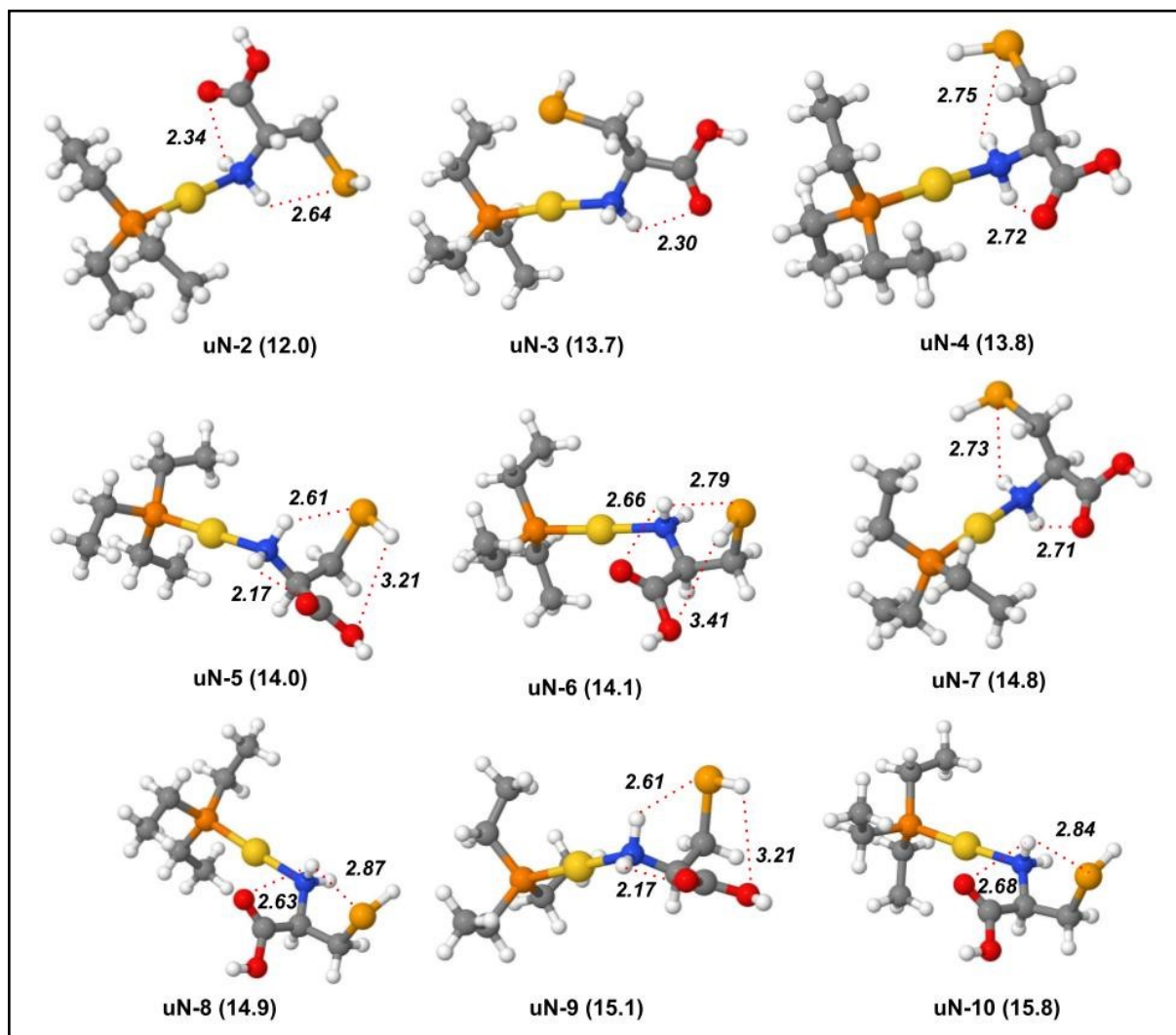
Figure S6: Optimized geometries of the most stable **uN** conformers of the $[(Et_3P)AuSec]^+$ ion, computed in gas phase at B3LYP/BS1 level of theory. Free energy values relative to **uSe-1** are reported in parenthesis in kJ mol^{-1}. Hydrogen bond distances (Å) are indicated by red dotted lines.
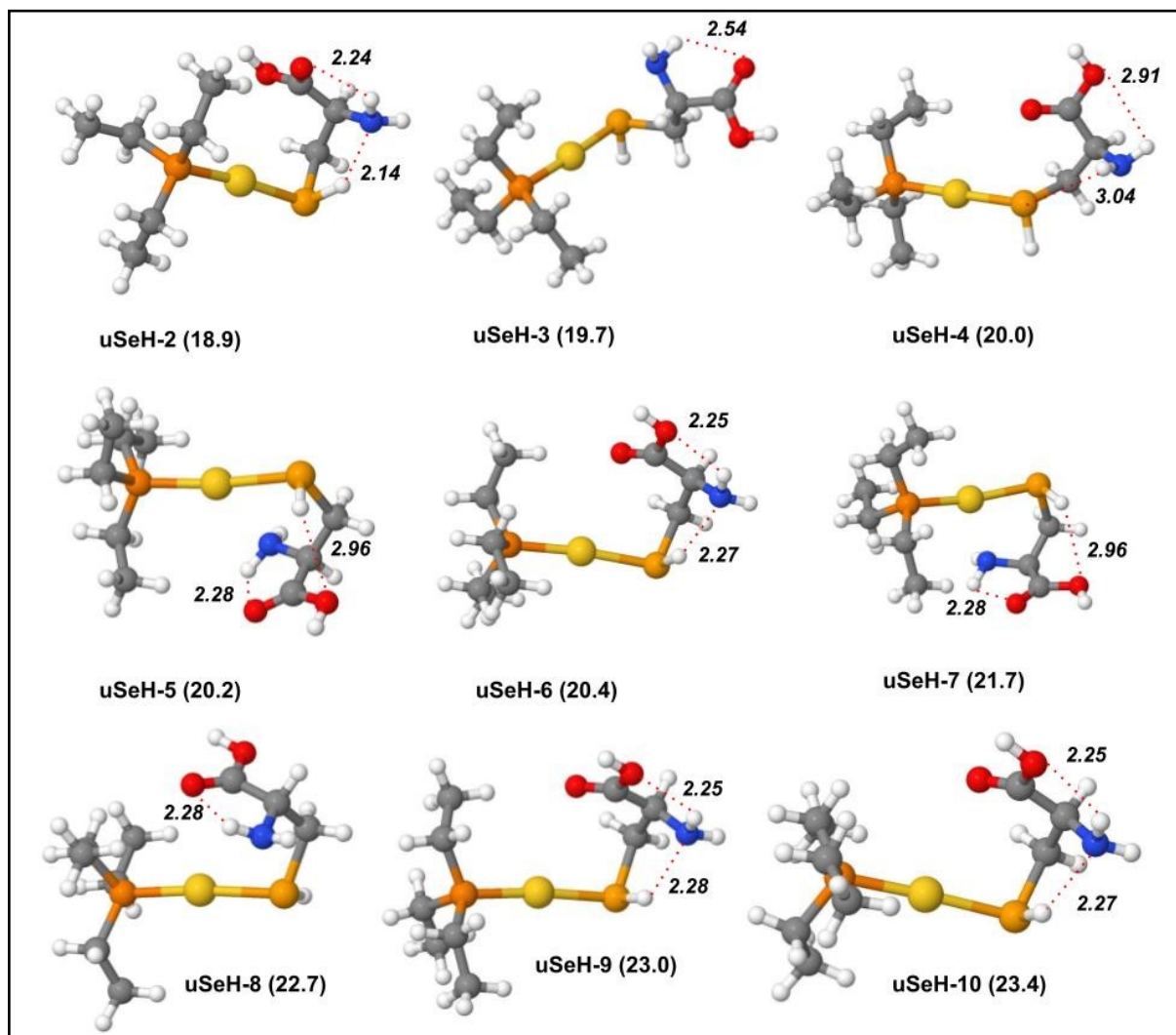
Figure S7: Optimized geometries of the most stable **uSeH** conformers of the [(Et$_3$P)AuSec]$^+$ ion, computed in gas phase at B3LYP/BS1 level of theory. Free energy values relative to **uSe-1** are reported in parenthesis in kJ mol^{-1}. Hydrogen bond distances (Å) are indicated by red dotted lines.
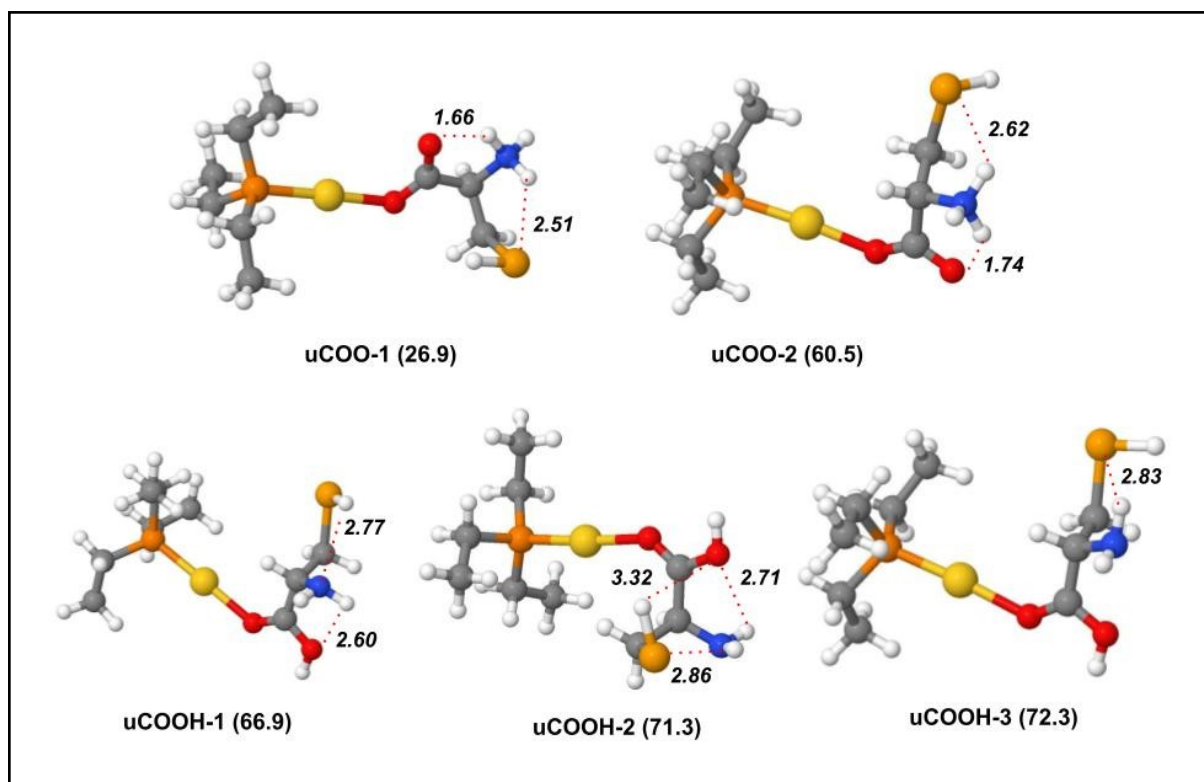
Figure S8: Optimized geometries of the most stable conformers of **uCOO** and **uCOOH** isomers for the [(Et₃P)AuSec]⁺ ion, computed in gas phase at B3LYP/BS1 level of theory. Free energy values relative to **uSe-1** are reported in parenthesis in kJ mol⁻¹. 5Hydrogen bond distances (Å) are indicated by red dotted lines.
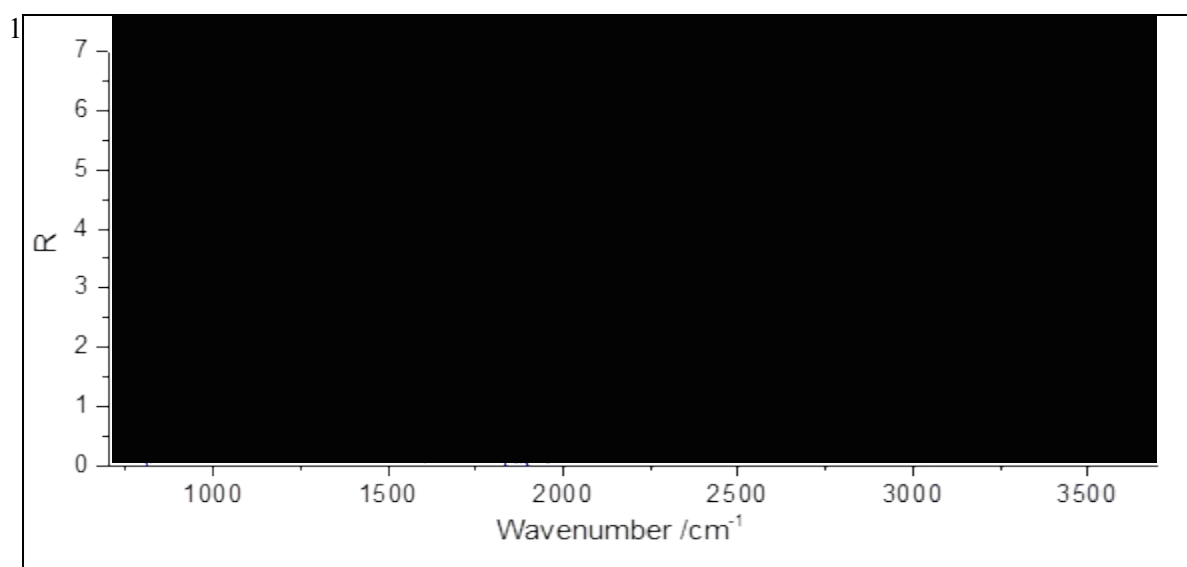
Figure S9: IRMPD spectrum of [(Et₃P)AuSec]⁺.
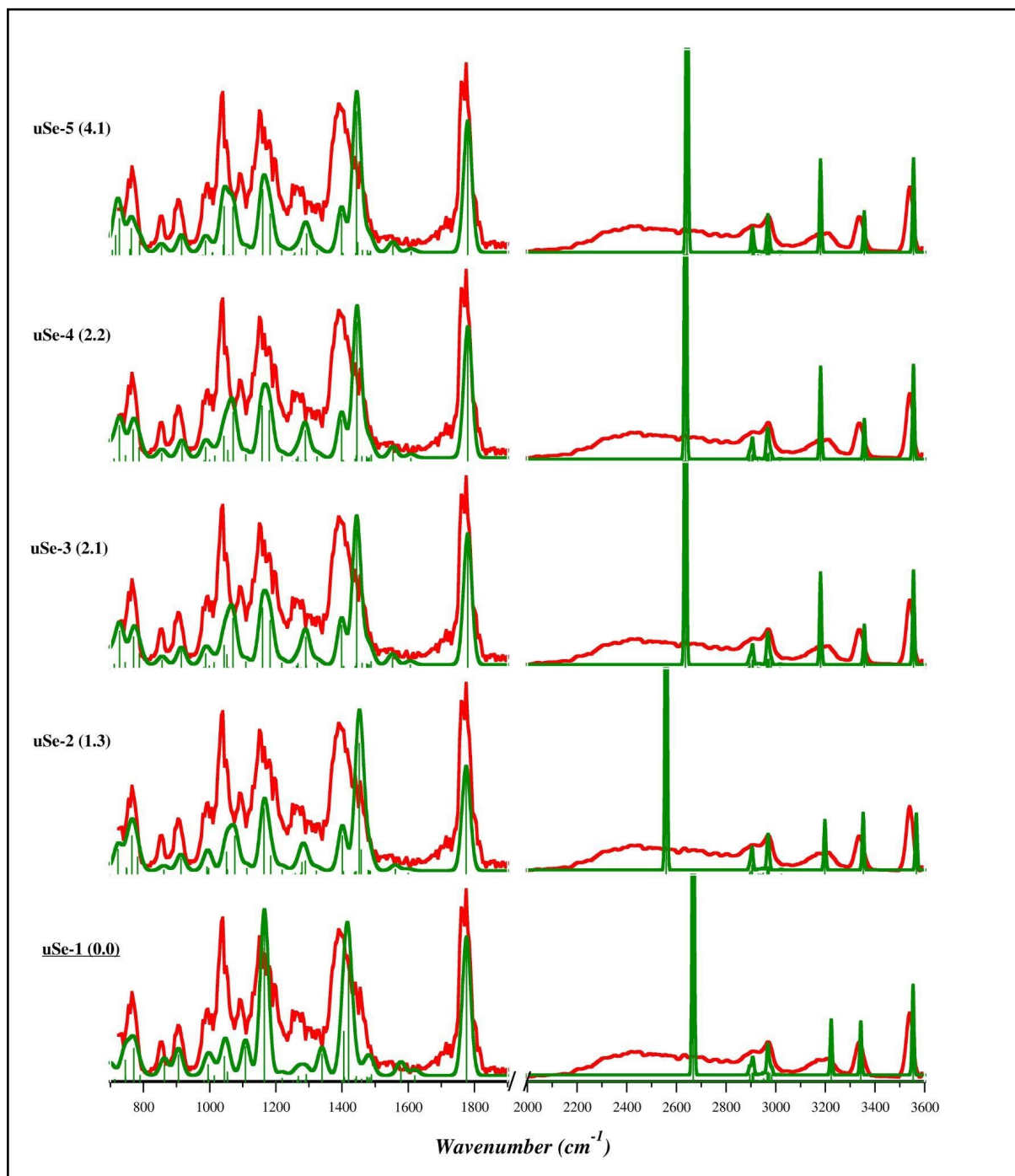
Figure S10: IRMPD spectrum (red profile) of $[(Et_3P)AuSec]^+$ ion and calculated harmonic IR spectra (green profiles) of the lowest lying conformers of **uSe** isomer, computed at the B3LYP/BS1 level of theory. Free energies relative to **uSe-1** are reported in brackets (kJ mol^{-1}). Harmonic frequencies computed in the 900−1900 and 2000-3600 cm^{-1} ranges were scaled by 0.985 and 0.955, respectively.
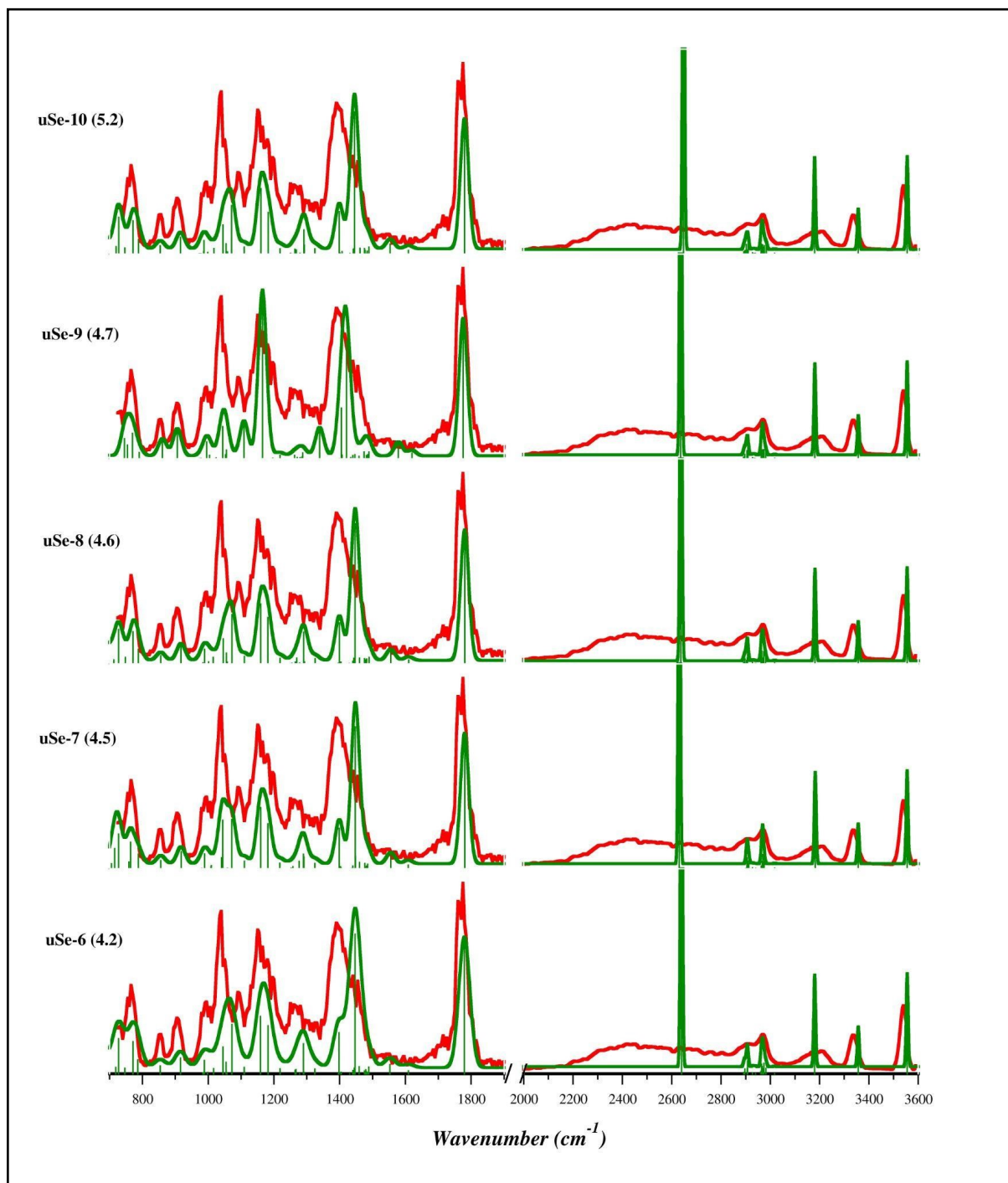
Figure S11: IRMPD spectrum (red profile) of $[(Et_3P)AuSec]^+$ ion and calculated harmonic IR spectra (green profiles) of the lowest lying conformers of **uSe** isomer, computed at the B3LYP/BS1 level of theory. Free energies relative to **uSe-1** are reported in brackets (kJ mol^{-1}). Harmonic frequencies computed in the 900−1900 and 2000-3600 cm^{-1} ranges were scaled by 0.985 and 0.955, respectively.
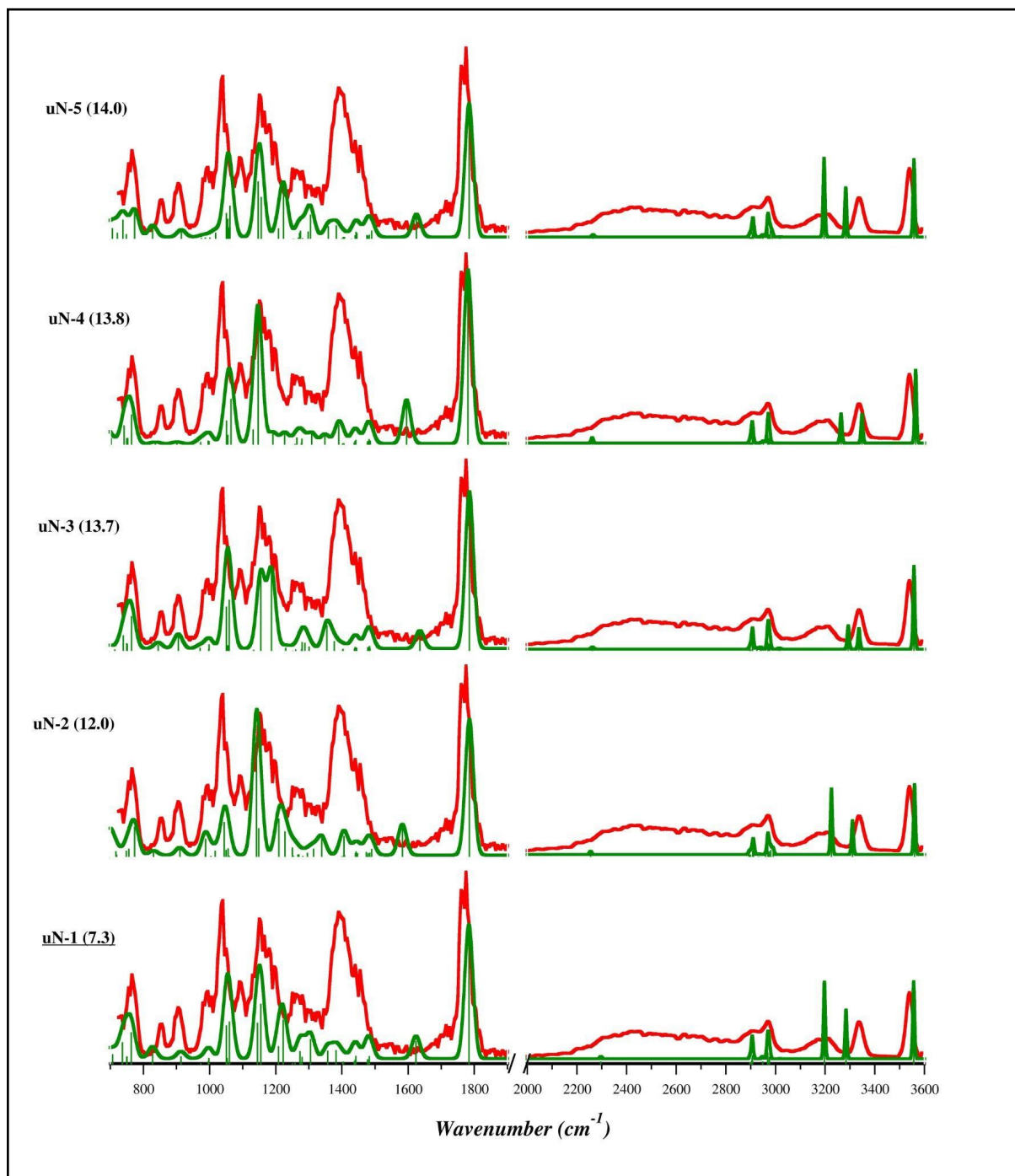
Figure S12: IRMPD spectrum (red profile) of $[(Et_3P)AuSec]^+$ ion and calculated harmonic IR spectra (green profiles) of the lowest lying conformers of **uN** isomer, computed at the B3LYP/BS1 level of theory. Free energies relative to **uSe-1** are reported in brackets (kJ mol^{-1}). Harmonic frequencies computed in the 900−1900 and 2000-3600 cm^{-1} ranges were scaled by 0.985 and 0.955, respectively.
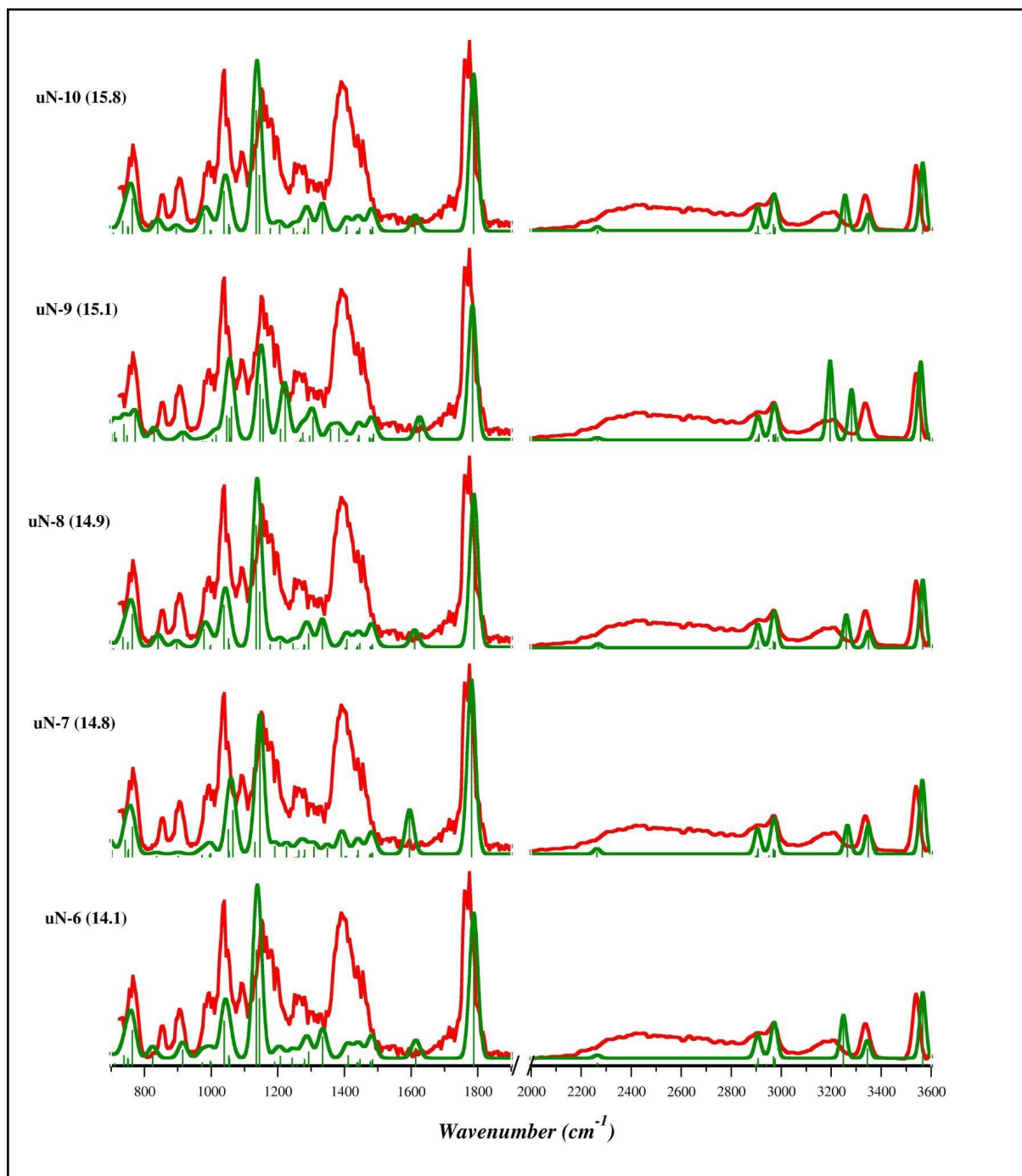
Figure S13: IRMPD spectrum (red profile) of [(Et$_3$P)AuSec]$^+$ ion and calculated harmonic IR spectra (green profiles) of the lowest lying conformers of **uN** isomer, computed at the B3LYP/BS1 level of theory. Free energies relative to **uSe-1** are reported in brackets (kJ mol^{-1}). Harmonic frequencies computed in the 900−1900 and 2000-3600 cm^{-1} ranges were scaled by 0.985 and 0.955, respectively.
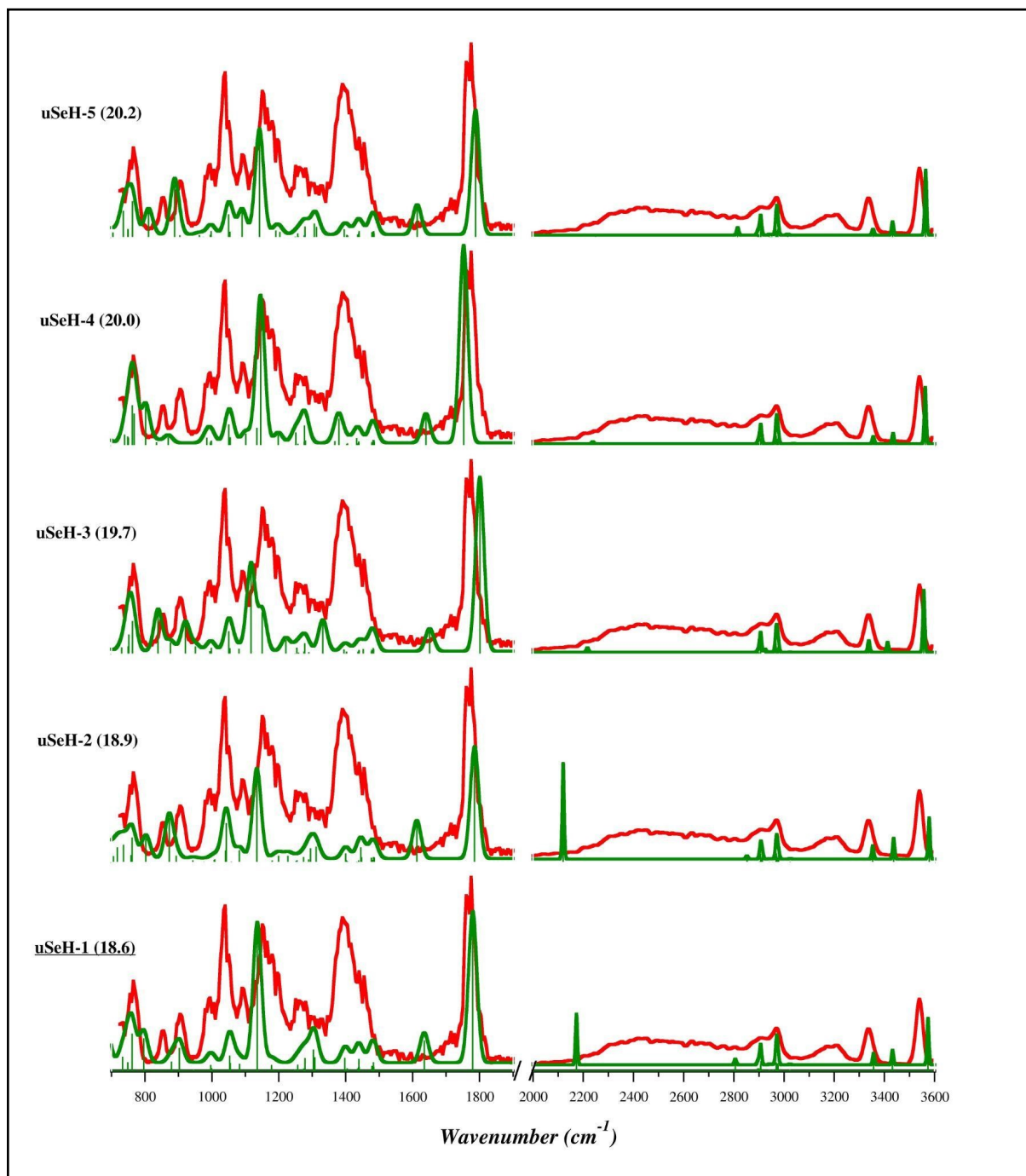
Figure S14: IRMPD spectrum (red profile) of [(Et$_3$P)AuSec]$^+$ ion and calculated harmonic IR spectra (green profiles) of the lowest lying conformers of **uSeH** isomer, computed at the B3LYP/BS1 level of theory. Free energies relative to **uSe-1** are reported in brackets (kJ mol^{-1}). Harmonic frequencies computed in the 900−1900 and 2000-39600 cm^{-1} ranges were scaled by 0.985 and 0.955, respectively.
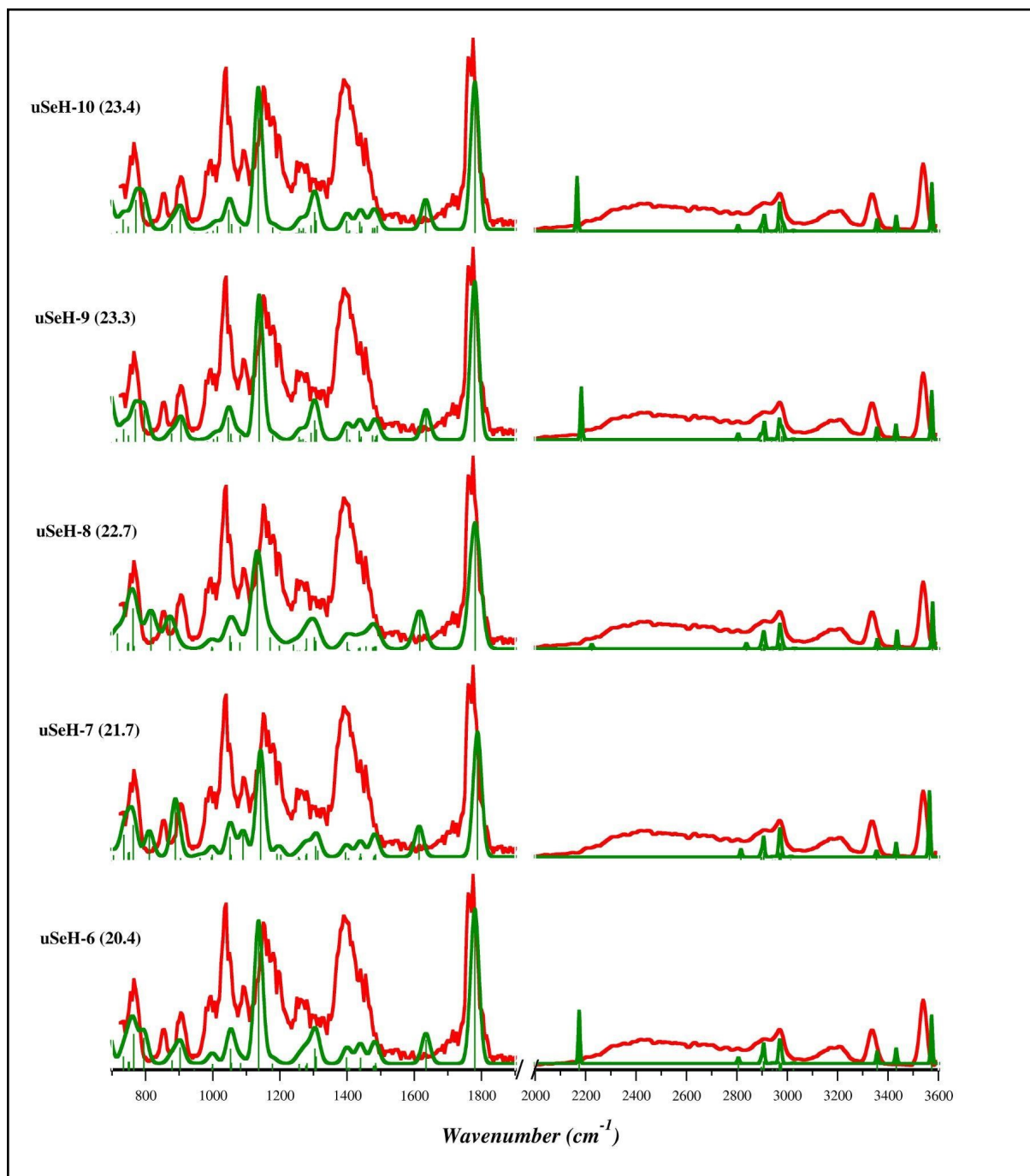
Figure S15: IRMPD spectrum (red profile) of [(Et$_3$P)AuSec]$^+$ ion and calculated harmonic IR spectra (green profiles) of the lowest lying conformers of **uSeH** isomer, computed at the B3LYP/BS1 level of theory. Free energies relative to **uSe-1** are reported in brackets (kJ mol^{-1}). Harmonic frequencies computed in the 900−1900 and 2000-3600 cm^{-1} ranges were scaled by 0.985 and 0.955, respectively.
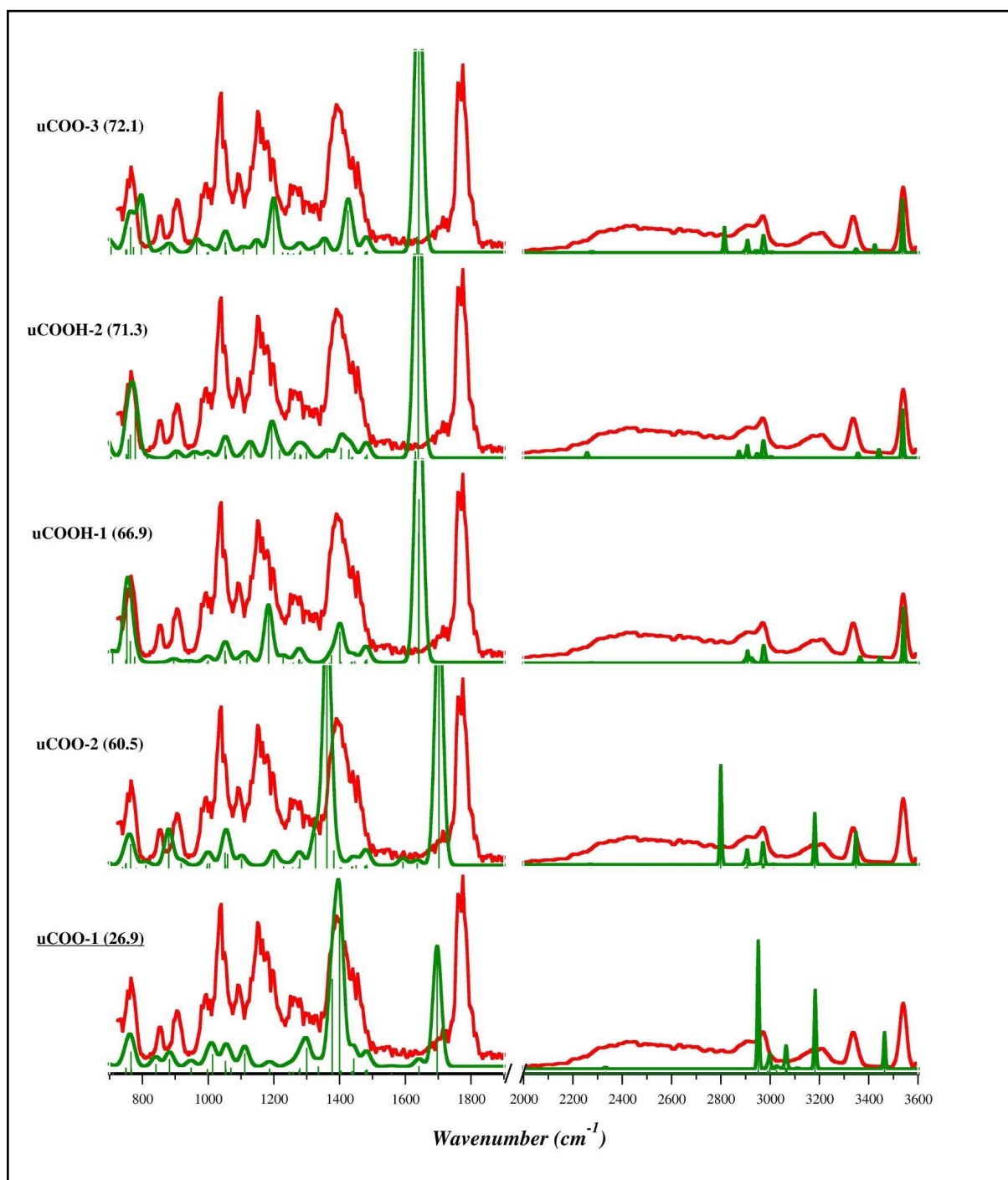
Figure S16: IRMPD spectrum (red profile) of $[(Et_3P)AuSec]^+$ ion and calculated harmonic IR spectra (green profiles) of the lowest lying conformers of **uCOOH** and **uCOO** isomers, computed at the B3LYP/BS1 level of theory. Free energies relative to **uSe-1** are reported in brackets (kJ mol^{-1}). Harmonic frequencies computed in the 900−1900 and 2000-3600 cm^{-1} ranges were scaled by 0.985 and 0.955, respectively.
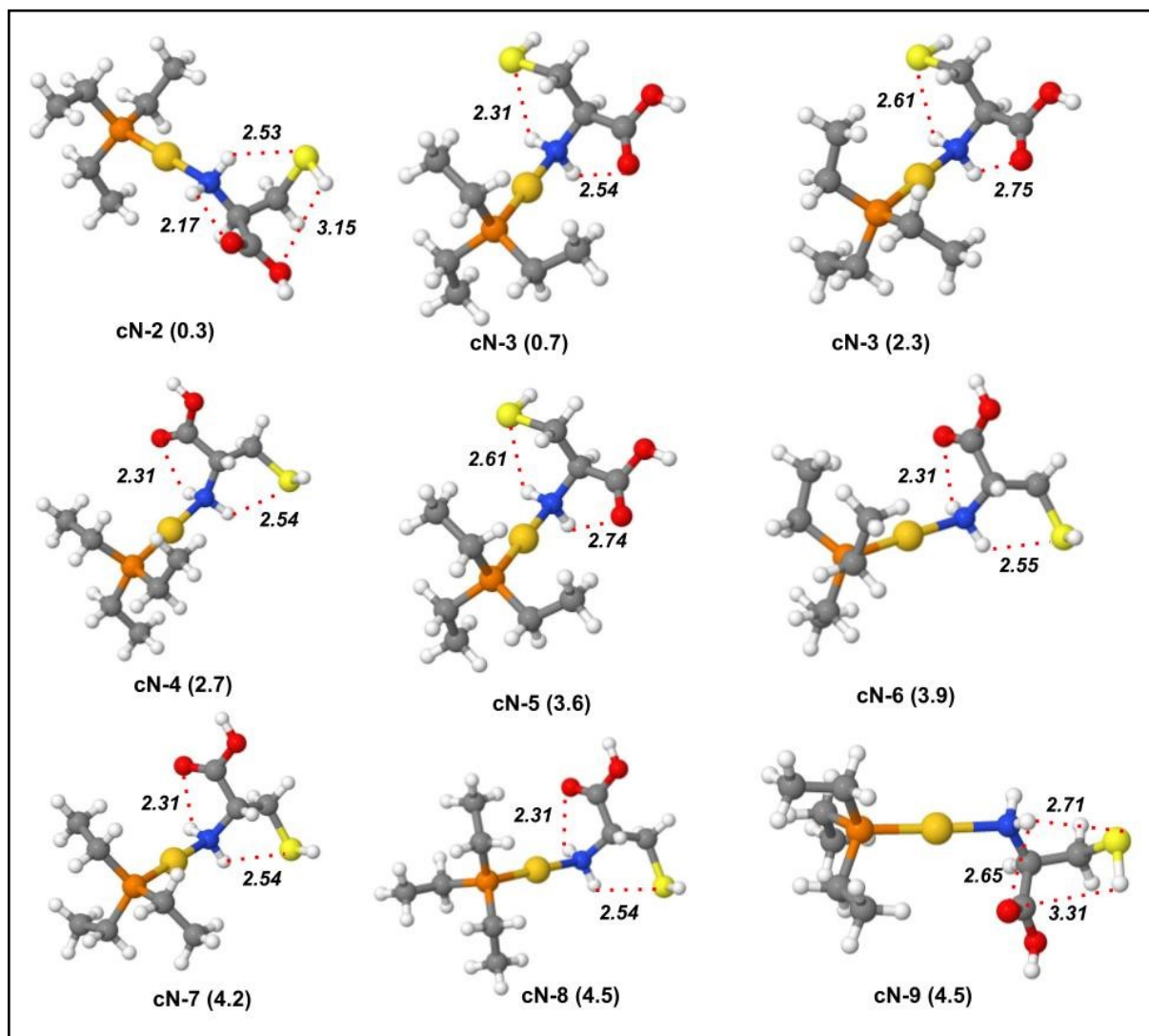
Figure S17: Optimized geometries of the most stable **cN** conformers of the $[(Et_3P)AuCys]^+$ ion, computed in gas phase at B3LYP/BS1 level of theory. Free energy values relative to **cN-1** are reported in parenthesis in kJ mol^{-1}. Hydrogen bond distances (Å) are indicated by red dotted lines.
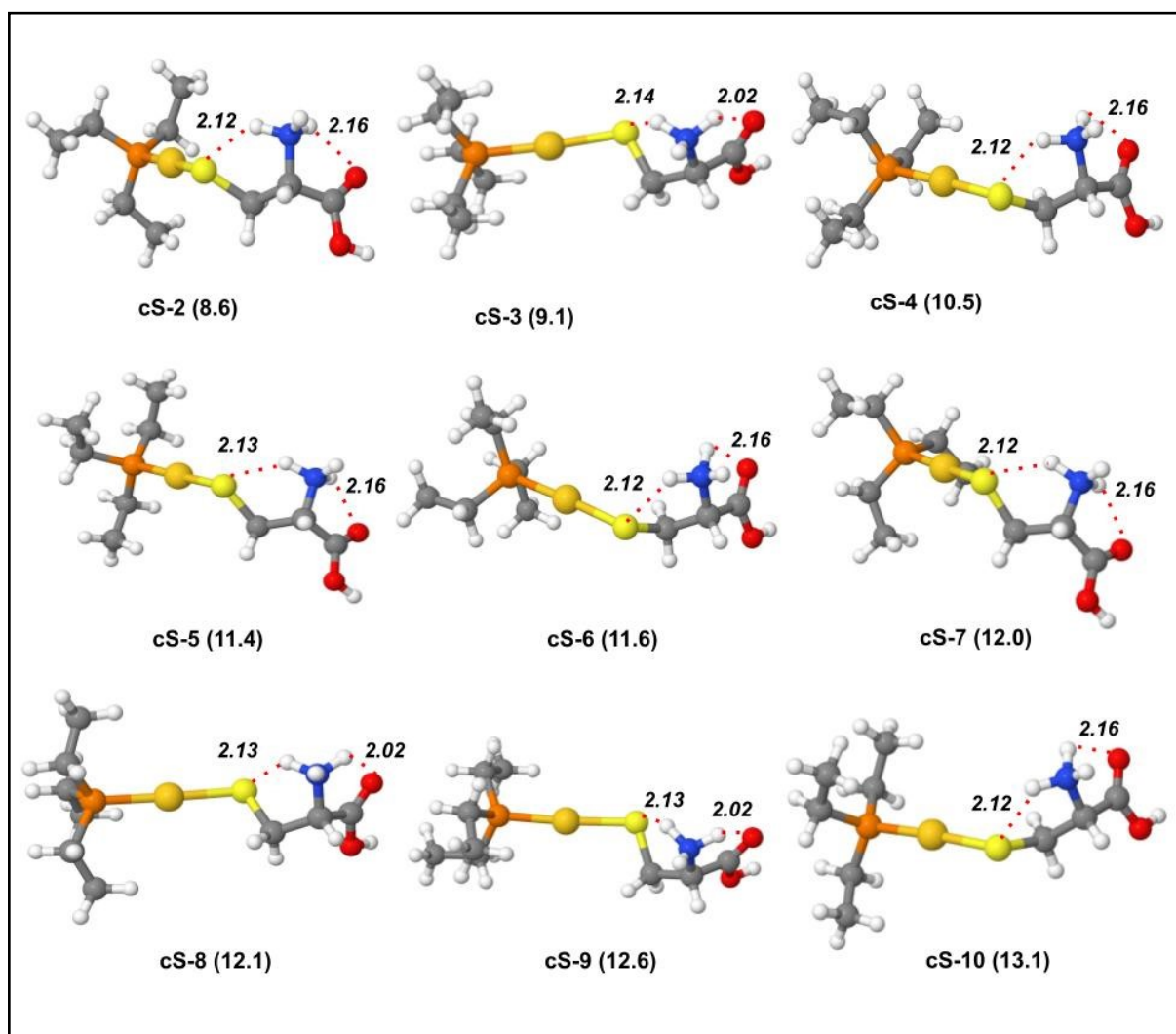
Figure S18: Optimized geometries of the most stable **cS** conformers of the [(Et₃P)AuCys]⁺ ion, computed in gas phase at B3LYP/BS1 level of theory. Free energy values relative to **cN-1** are reported in parenthesis in kJ mol⁻¹. Hydrogen bond distances (Å) are indicated by red dotted lines.
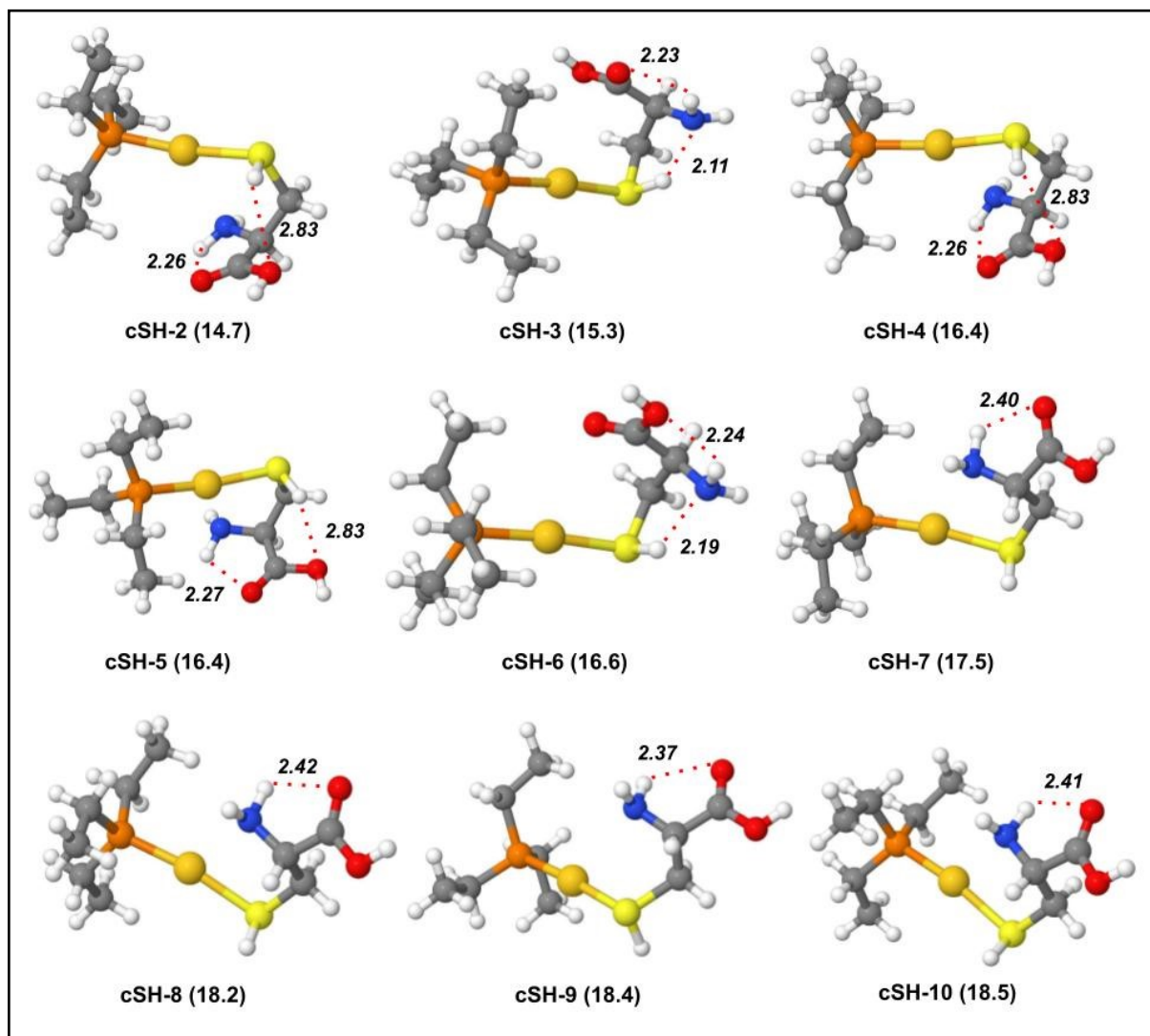
Figure S19: Optimized geometries of the most stable **cSH** conformers of the [(Et$_3$P)AuCys]$^+$ ion, computed in gas phase at B3LYP/BS1 level of theory. Free energy values relative to **cN-1** are reported in parenthesis in kJ mol^{-1}. Hydrogen bond distances (Å) are indicated by red dotted lines.
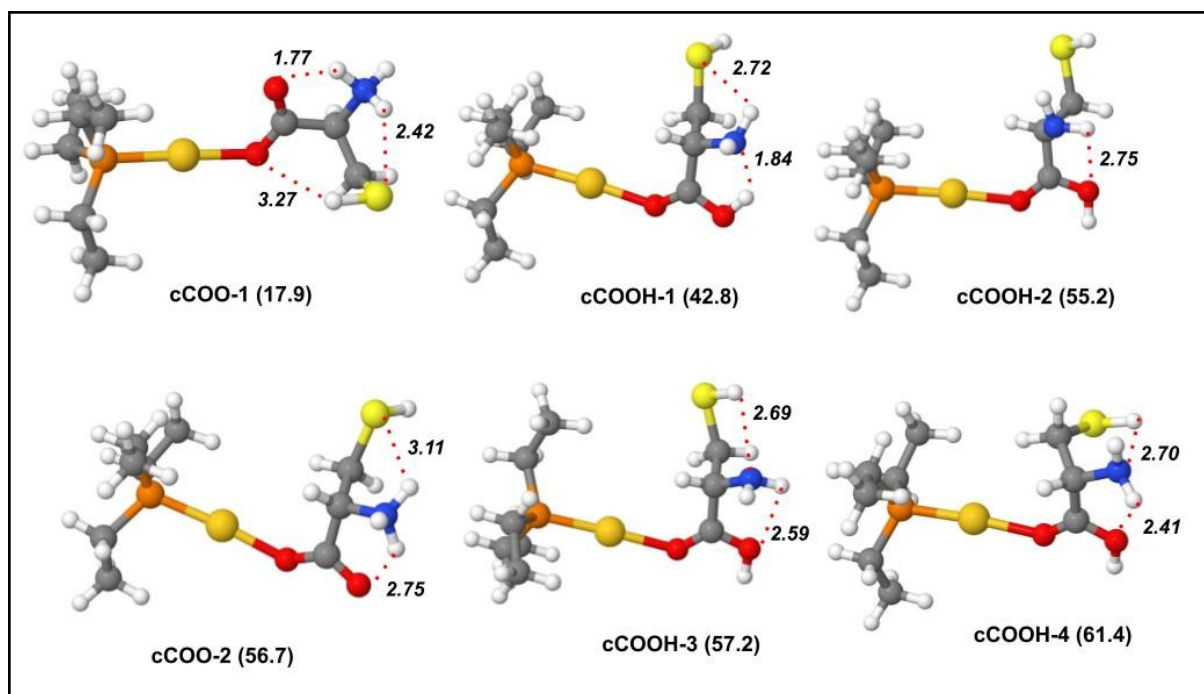
Figure S20: Optimized geometries of the most stable conformers of **cCOO** and **cCOOH** isomers for the [(Et$_3$P)AuCys]$^+$ ion, computed in gas phase at B3LYP/BS1 level of theory. Free energy values relative to **cN-1** are reported in parenthesis in kJ mol^{-1}. Hydrogen bond distances (Å) are indicated by red dotted lines.
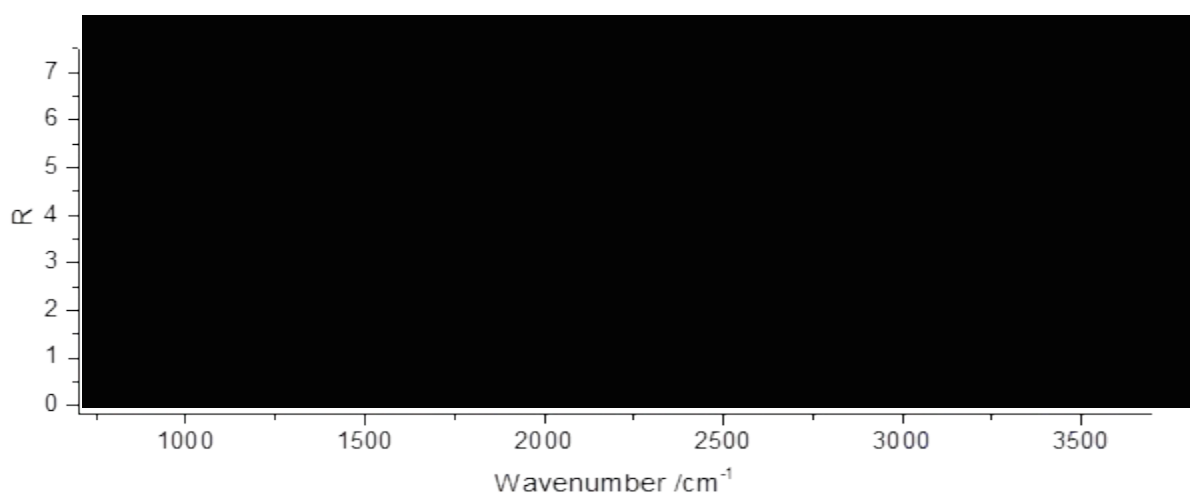
Figure S21: IRMPD spectrum of [(Et$_3$P)AuCys]$^+$.
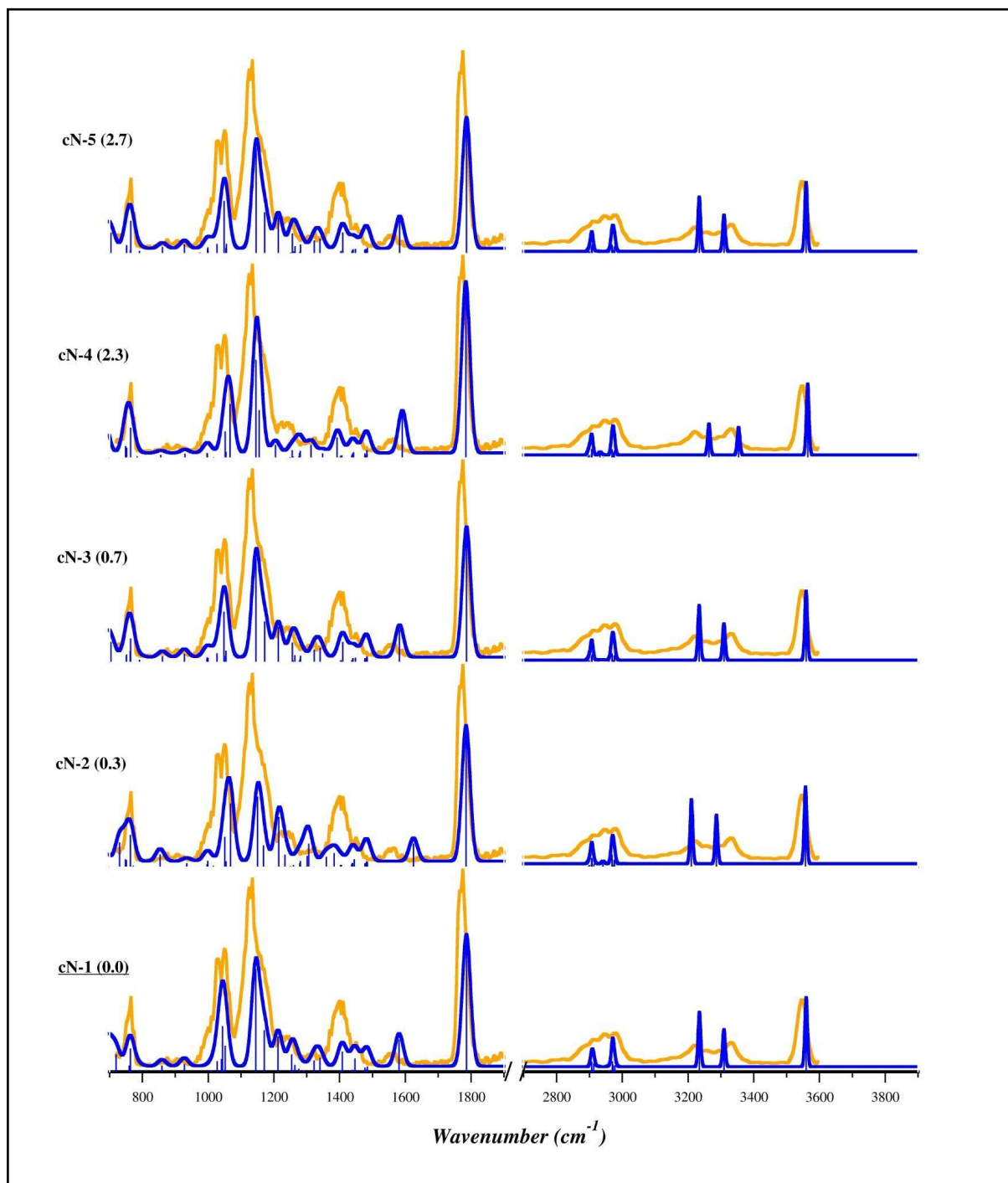
Figure S22: IRMPD spectrum (orange profile) of $[(Et_3P)AuCys]^+$ ion and calculated harmonic IR spectra (blue profiles) of the lowest lying conformers of **cN** isomer, computed at the B3LYP/BS1 level of theory. Free energies relative to **cN-1** are reported in brackets (kJ mol^{-1}). Harmonic frequencies computed in the 900−1900 and 2700-3900 cm^{-1} ranges were scaled by 0.985 and 0.955, respectively.
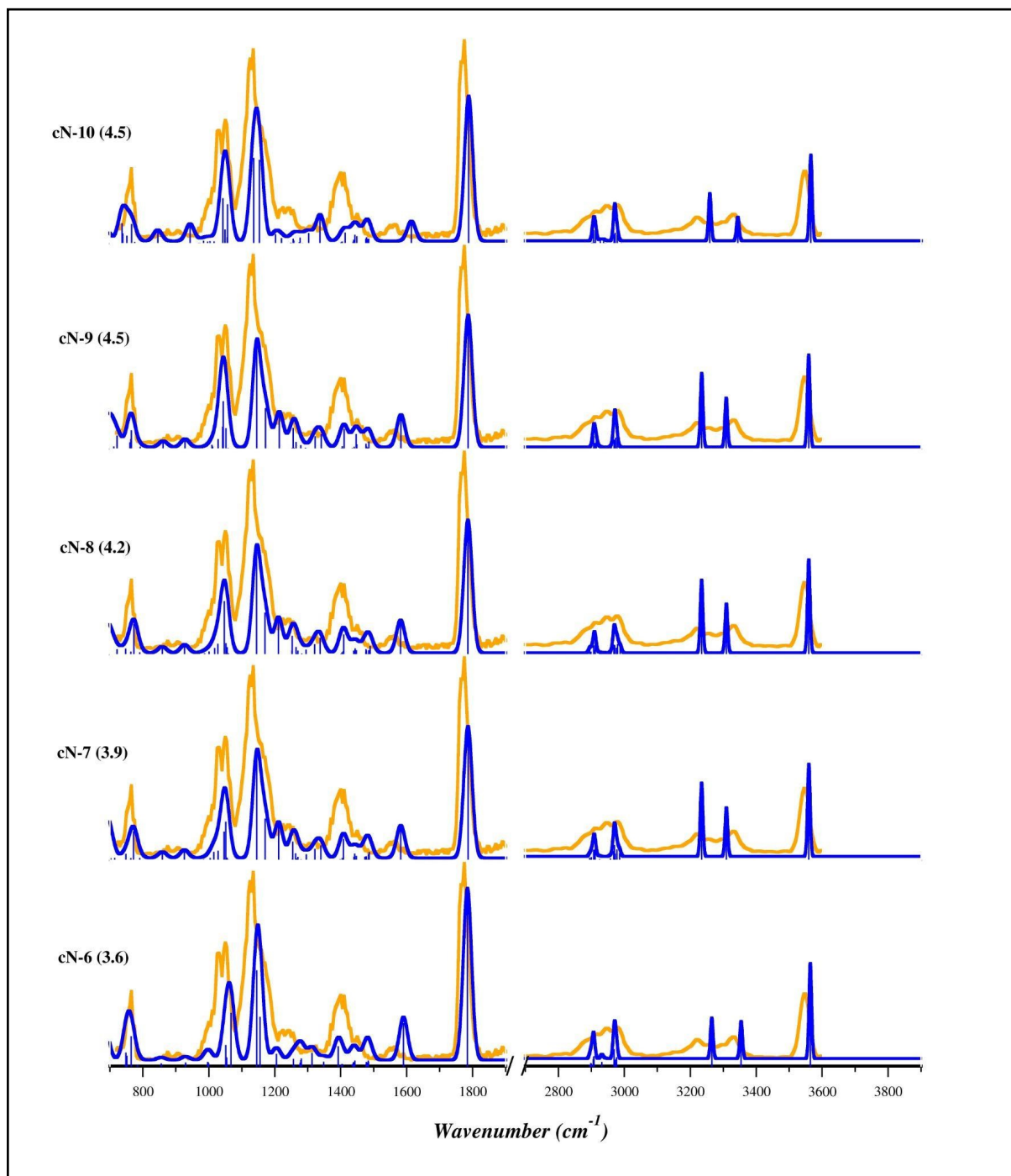
Figure S23: IRMPD spectrum (orange profile) of $[(Et_3P)AuCys]^+$ ion and calculated harmonic IR spectra (blue profiles) of the lowest lying conformers of **cN** isomer, computed at the B3LYP/BS1 level of theory. Free energies relative to **cN-1** are reported in brackets (kJ mol^{-1}). Harmonic frequencies computed in the 900−1900 and 2700-3900 cm^{-1} ranges were scaled by 0.985 and 0.955, respectively.
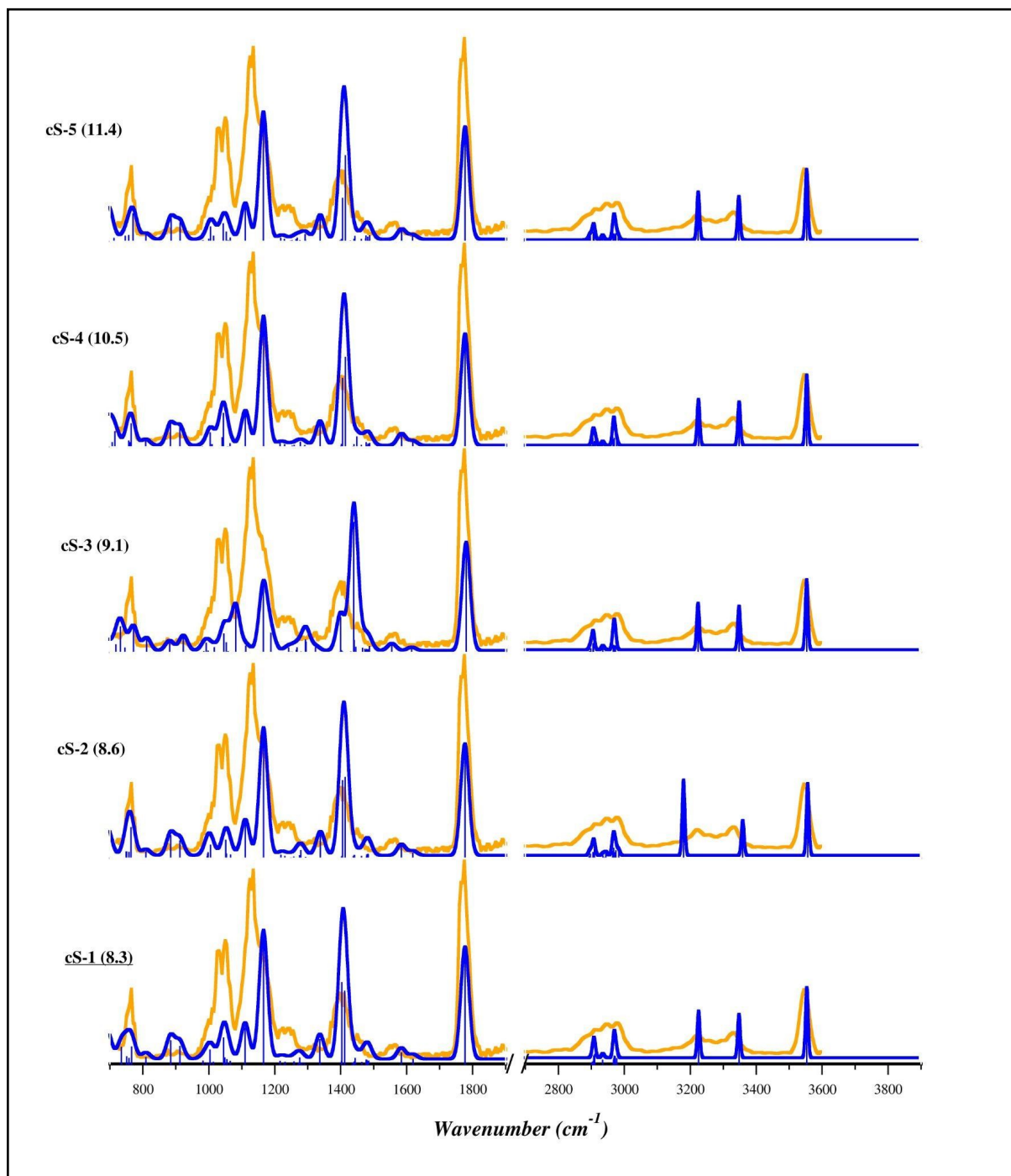
Figure S24: IRMPD spectrum (orange profile) of [(Et$_3$P)AuCys]$^+$ ion and calculated harmonic IR spectra (blue profiles) of the lowest lying conformers of **cS** isomer, computed at the B3LYP/BS1 level of theory. Free energies relative to **cN-1** are reported in brackets (kJ mol^{-1}). Harmonic frequencies computed in the 900−1900 and 2700-3900 cm^{-1} ranges were scaled by 0.985 and 0.955, respectively.
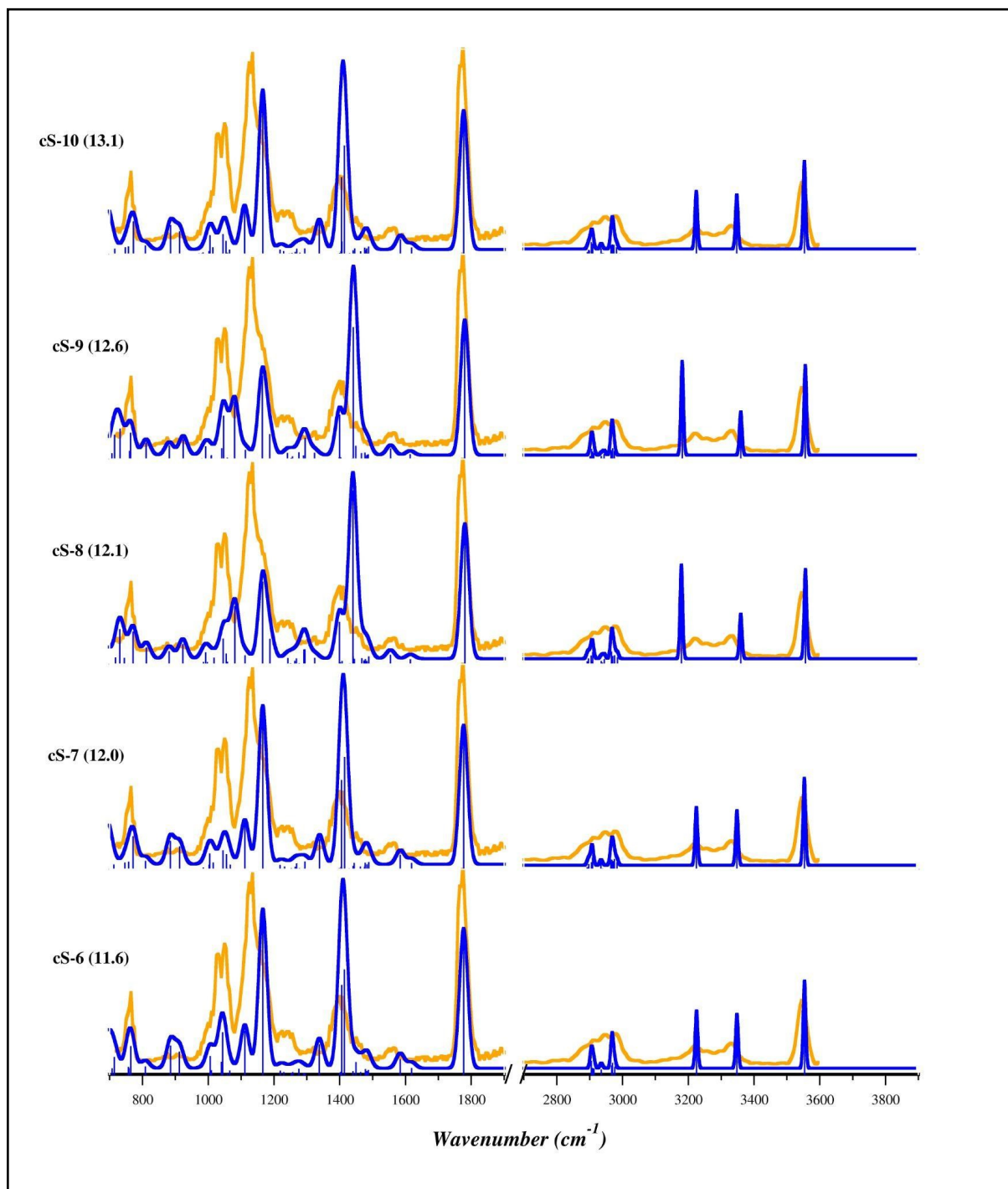
Figure S25: IRMPD spectrum (orange profile) of $[(Et_3P)AuCys]^+$ ion and calculated harmonic IR spectra (blue profiles) of the lowest lying conformers of **cS** isomer, computed at the B3LYP/BS1 level of theory. Free energies relative to **cN-1** are reported in brackets (kJ mol^{-1}). Harmonic frequencies computed in the 900−1900 and 2700-3900 cm^{-1} ranges were scaled by 0.985 and 0.955, respectively.
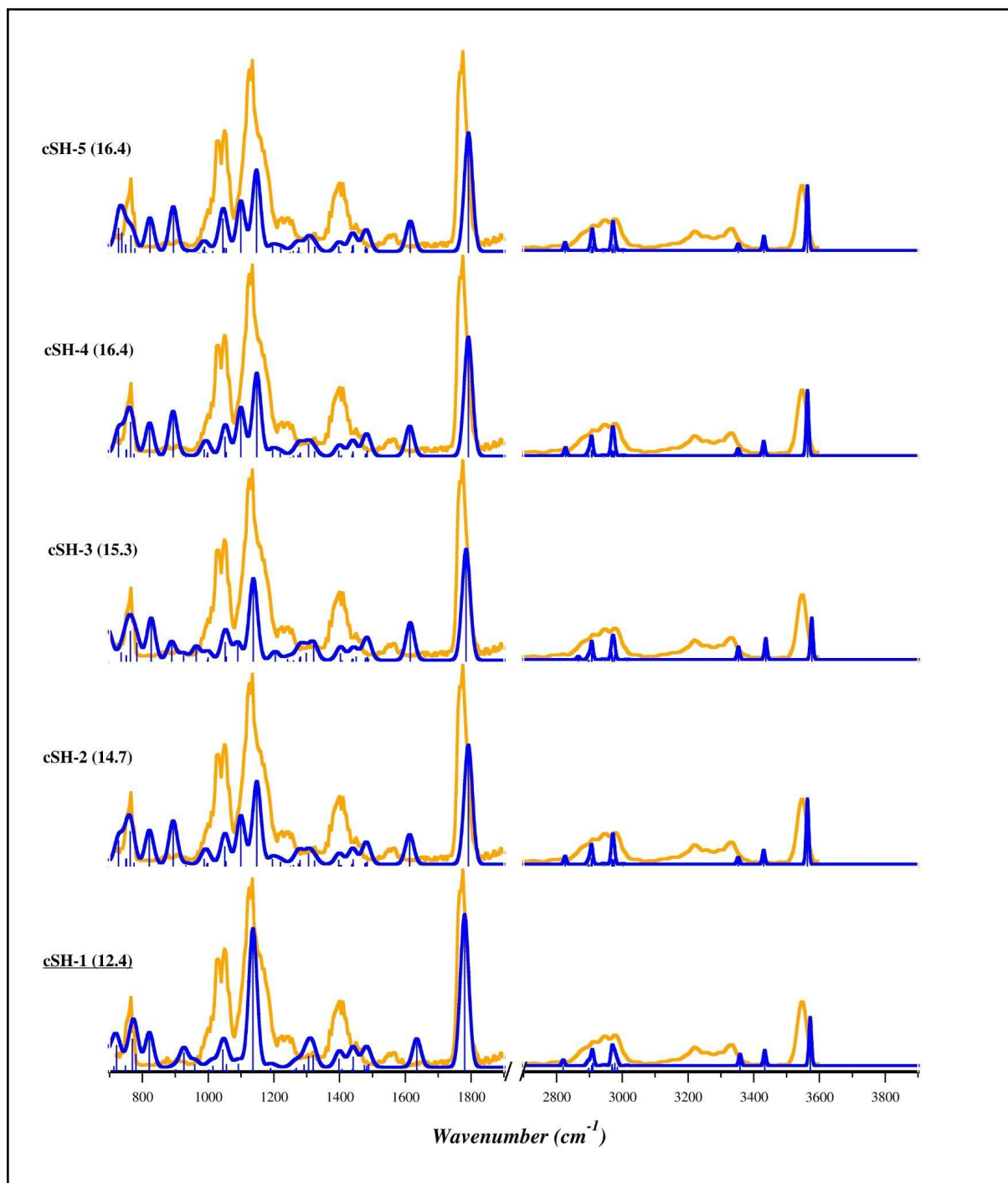
Figure S26: IRMPD spectrum (orange profile) of $[(Et_3P)AuCys]^+$ ion and calculated harmonic IR spectra (blue profiles) of the lowest lying conformers of **cSH** isomer, computed at the B3LYP/BS1 level of theory. Free energies relative to **cN-1** are reported in brackets (kJ mol^{-1}). Harmonic frequencies computed in the 900−1900 and 2700-3900 cm^{-1} ranges were scaled by 0.985 and 0.955, respectively.
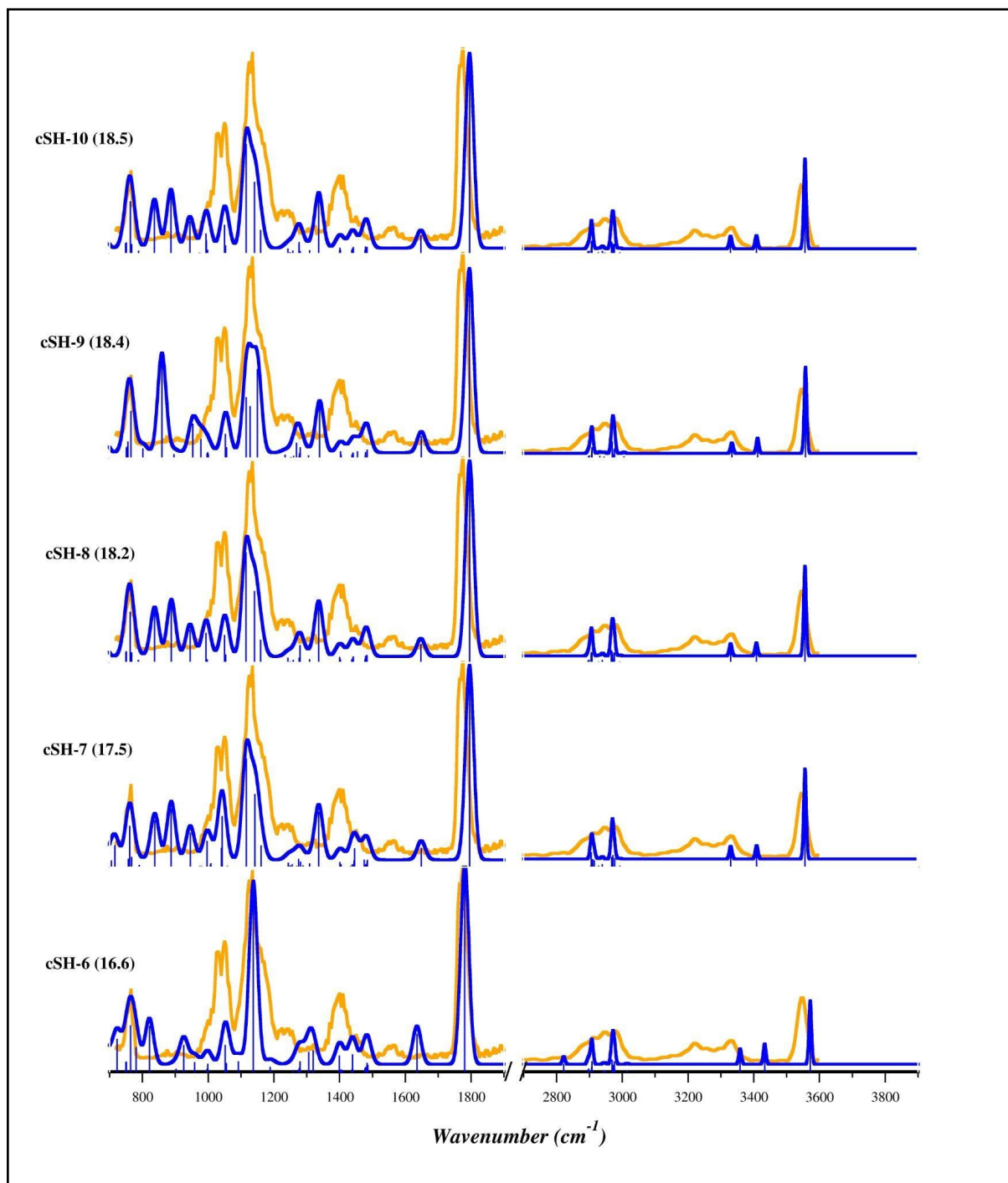
Figure S27: IRMPD spectrum (orange profile) of $[(Et_3P)AuCys]^+$ ion and calculated harmonic IR spectra (blue profiles) of the lowest lying conformers of **cSH** isomer, computed at the B3LYP/BS1 level of theory. Free energies relative to **cN-1** are reported in brackets (kJ mol^{-1}). Harmonic frequencies computed in the 900−1900 and 2700-3900 cm^{-1} ranges were scaled by 0.985 and 0.955, respectively.
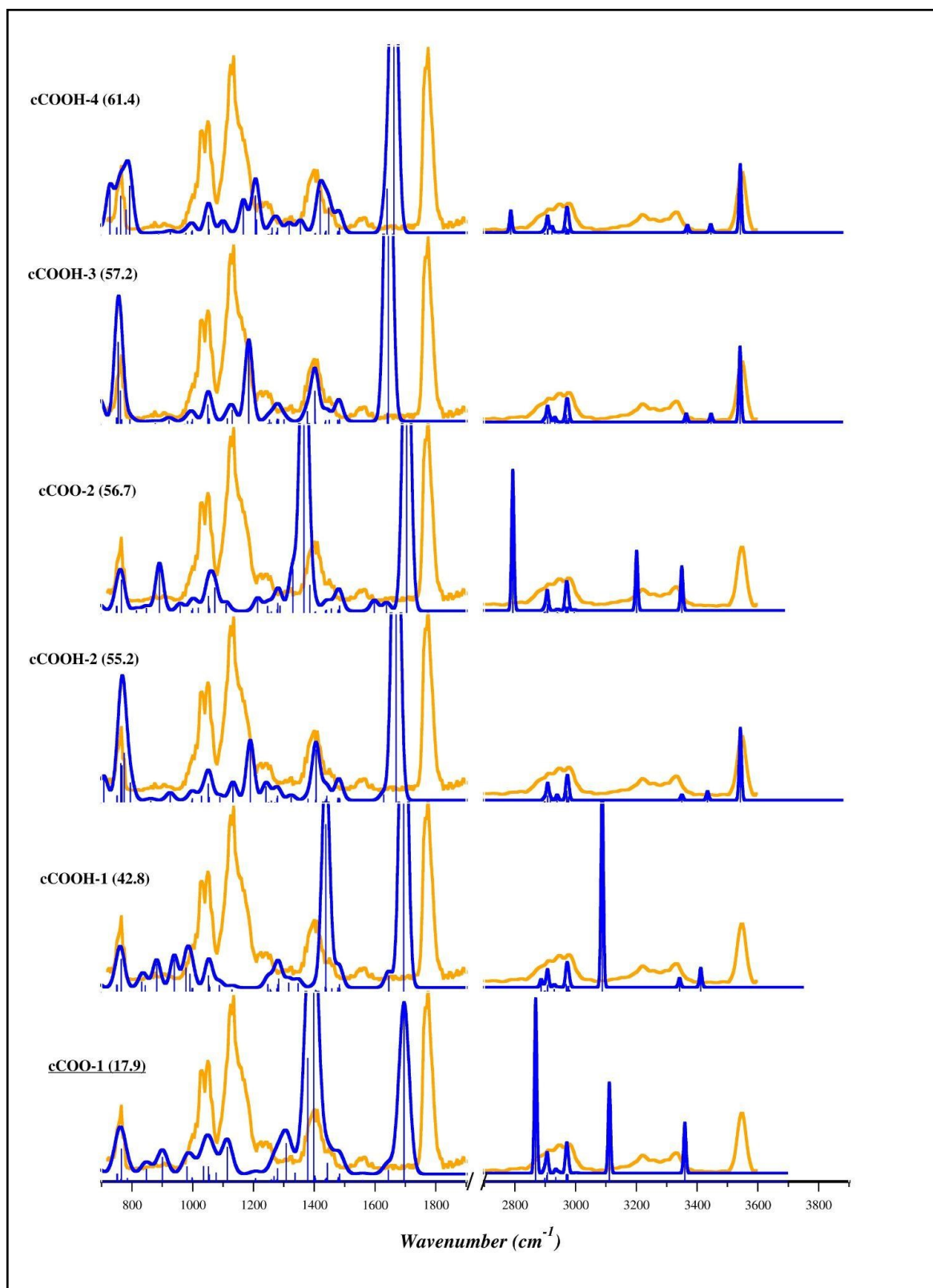
Figure S28: IRMPD spectrum (orange profile) of $[(Et_3P)AuCys]^+$ ion and calculated harmonic IR spectra (blue profiles) of the lowest lying conformers of **cCOOH** and **cCOO** isomers, computed at the B3LYP/BS1 level of theory. Free energies relative to **cN-1** are reported in brackets (kJ mol^{-1}). Harmonic frequencies computed in the 900−1900 and 2700-3900 cm^{-1} ranges were scaled by 0.985 and 0.955, respectively.
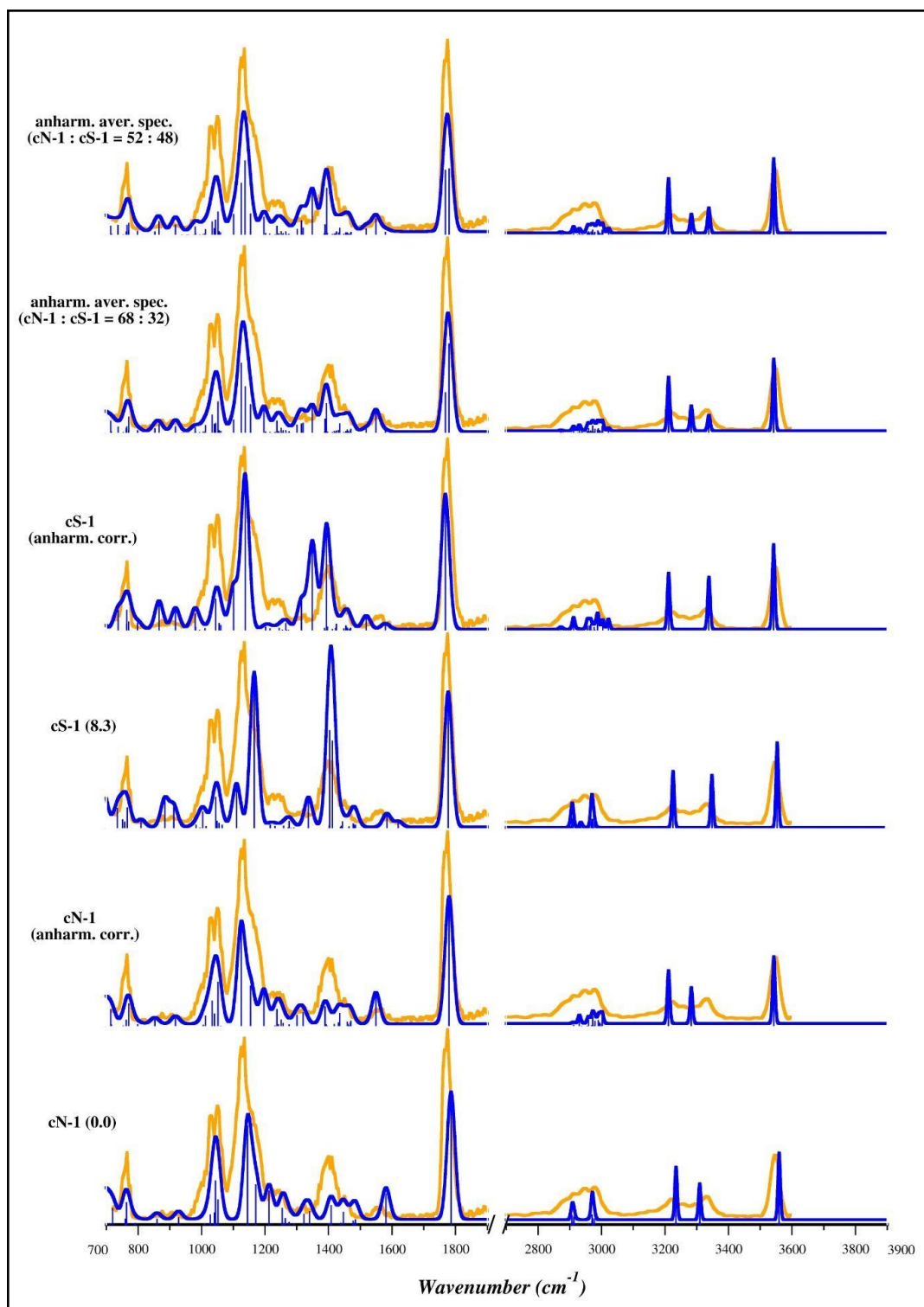
Figure S29: IRMPD spectrum (orange profile) of $[(Et_3P)AuCys]^+$ ion and calculated harmonic and anharmonic IR spectra (blue profiles) of **cN-1** and **cS-1**, computed at the B3LYP/BS1 level of theory. Free energies relative to **cN-1** are reported in brackets (kJ mol^{-1}). Harmonic frequencies computed in the 900−1900 and 2700-3900 cm^{-1} ranges were scaled by 0.985 and 0.955, respectively. The anharmonic averaged spectra are built by considering the contributions of **cN-1** and **cS-1** to the Boltzmann population weighted according to their relative free energy computed in 50:50 water-methanol mixture (see Table 1 for additional details).
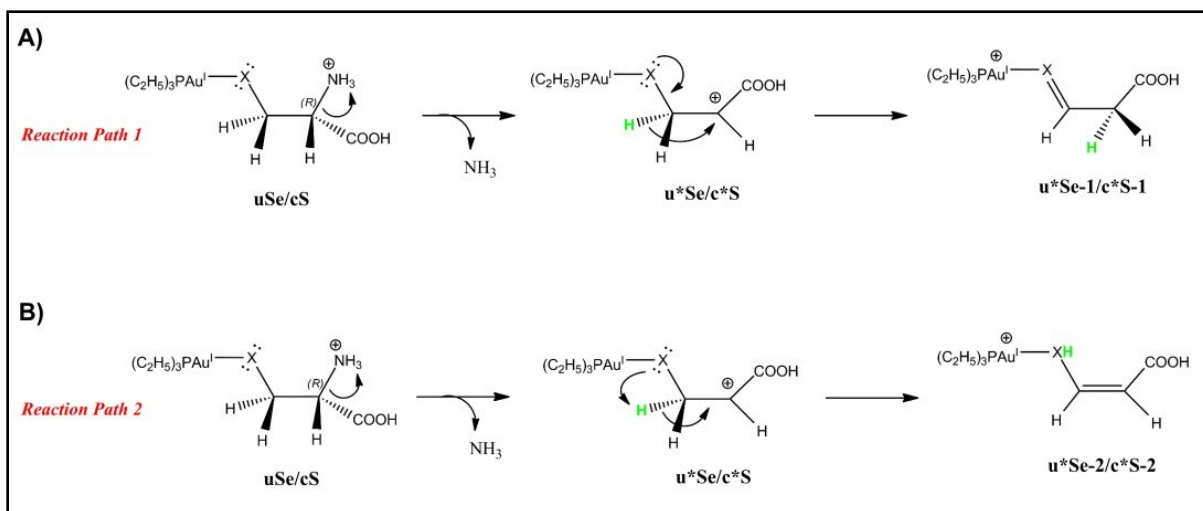
Figure S30: possible pathways for the deamination process of $[(Et_3P)AuSec]^+$ and $[(Et_3P)AuCys]^+$ ions in CID experiments leading to A) 3-sulfanylidenepropanoic acid or 3-selenylidenepropanoic acid derivatives (**u*Se-1** or **c*S-1**) and B) 3-selanylprop-2-enoic acid or 3-sulfanylprop-2-enoic acid derivatives (**u*Se-2** or **c*S-2**). X is the Se or S atom for $[(Et_3P)AuSec]^+$ and $[(Et_3P)AuCys]^+$, respectively.
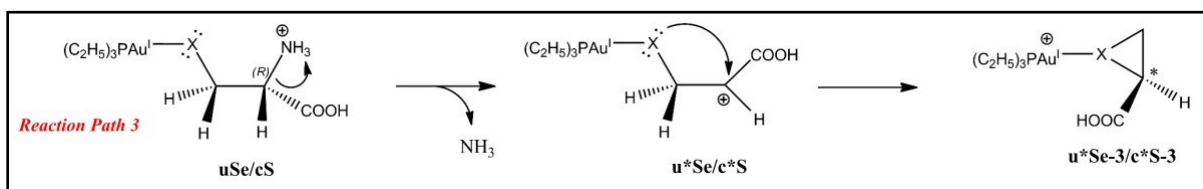
Figure S31: possible pathways for the deamination process of $[(Et_3P)AuSec]^+$ and $[(Et_3P)AuCys]^+$ ions in CID experiments leading to A) 1-(selanylcyclopropan-2-yl)methanoic acid or 1-(thiacyclopropan-2-yl)methanoic acid derivatives (**u*Se-1** or **c*S-1**).. X is the Se or S atom for $[(Et_3P)AuSec]^+$ and $[(Et_3P)AuCys]^+$, respectively.
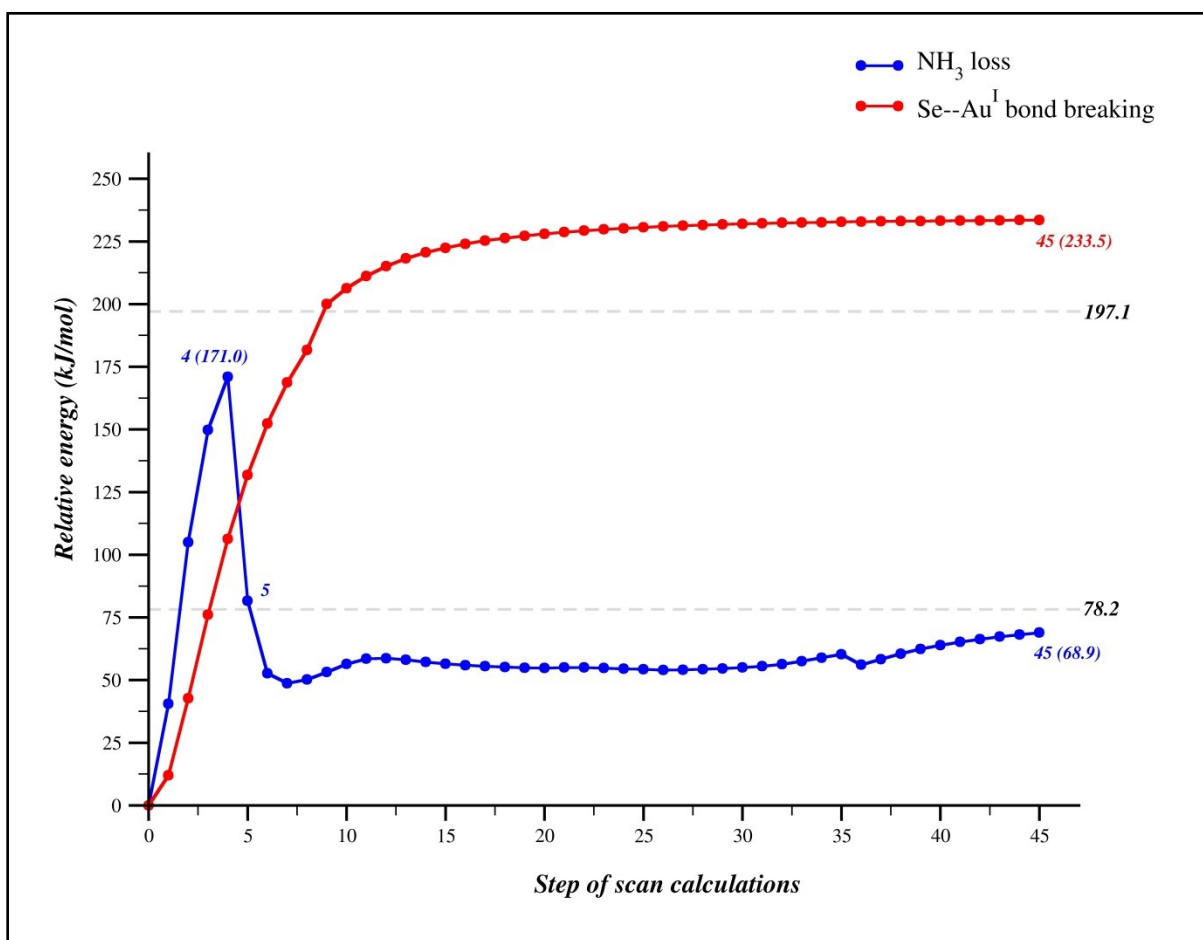
Figure S32: Relaxed potential energy scans for NH_3 loss (blue profile) and Se--Au^I bond breaking (red profile) as a function of the respective reaction coordinates: C_α-NH_3^+ (blue) and Au^I-Se (red) bond distances for **cSe-1**. The scan step was 0.25 Å for a total of 45 steps. Relative electronic energies of transition state and the last step are reported for both reaction paths. The reaction energy computed considering reactants and products at infinite distance are reported in black. Calculations were performed at the B3LYP level of theory using the B3LYP/6-311+G(d,p)//LANL2DZ basis set in the gas phase. The structures of step 4, 5, 45 (blue profile) and 45 (red profile) are reported in Figure S34 and S35, respectively.
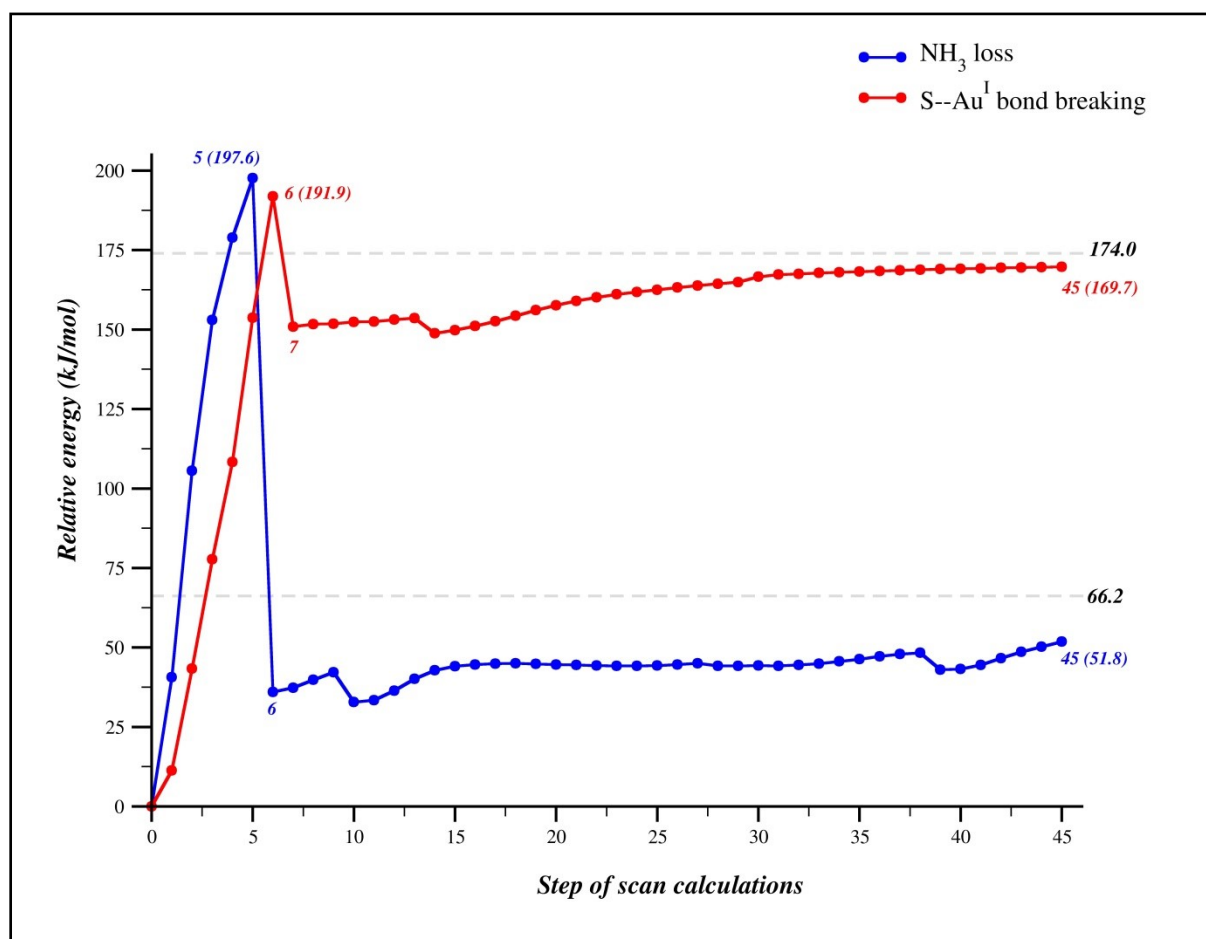
Figure S33: Relative electronic energies curves on NH_3 loss (blue profile) and S-Au^I bond breaking (red profile) reactions as a function of the C_α-NH_3^+ (blue profile) and Au^I-S (red profile) distances for **cS-1** obtained by relaxed scan calculations. The scan step was 0.25 Å for a total of 45 steps. Relative electronic energies of transition state and the last step are reported for both reaction paths. The reaction energy computed considering reactants and products at infinite distance are reported in black. Calculations were performed at the B3LYP level of theory using the B3LYP/6-311+G(d,p)/LANL2DZ basis set in the gas phase. The structures of step 5, 6, 45 (blue profile) and 6,7, 45 (red profile) are reported in Figure S36 and S37, respectively.
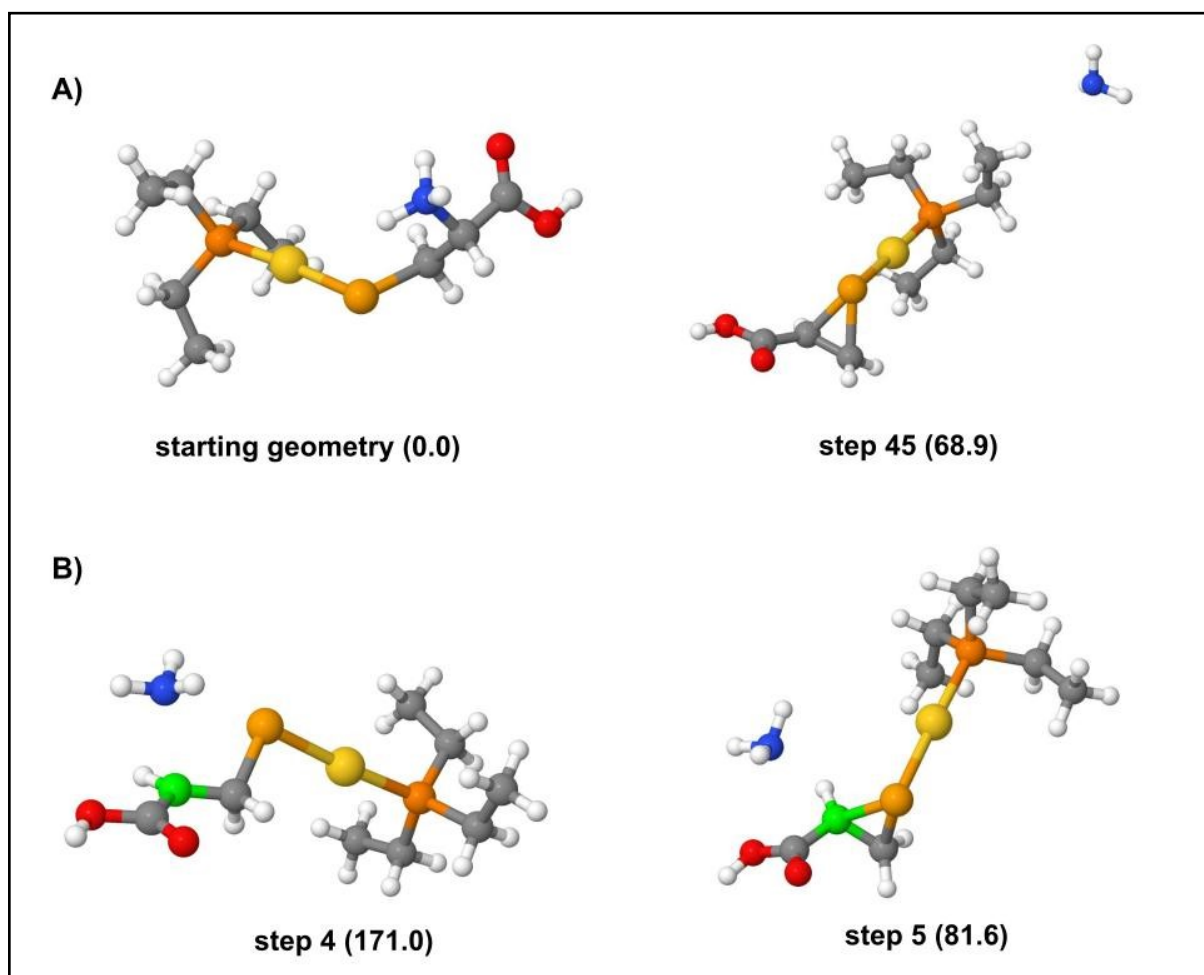
Figure S34: Most relevant optimized geometries of the relaxed scan calculations at the B3LYP/6-311+G(d,p)/LANL2DZ, computed for [(Et$_3$P)AuSec]$^+$ along the C$_\alpha$-NH$_3^+$ bond breaking reaction coordinate by using a step of 0.25 Å for a total of 45 steps (Figure S32, blue profile): A) optimized geometries of the first (**uSe-1**) and the last step (45) of scan calculation; B) optimized structures of highest energy step (step 4) and of the following one (step 5) along the reaction coordinate. The carbon C$_\alpha$ attacked by the Se atom is colored in green. Electron energies relative to the starting geometry (**uSe-1**) are reported in brackets (kJ mol^{-1}).
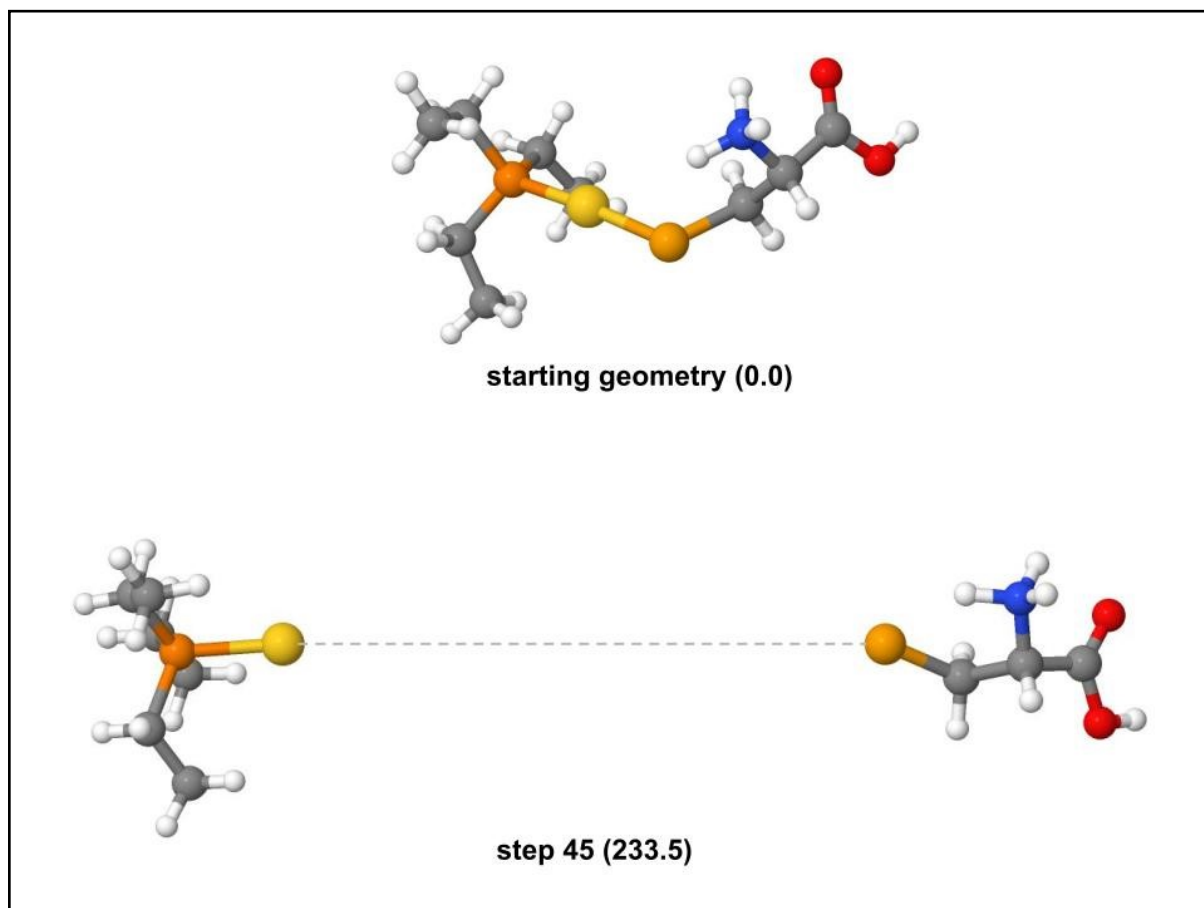
Figure S35: Most relevant optimized geometries of the relaxed scan calculations at the B3LYP/6-311+G(d,p)/LANL2DZ, computed for $[(Et_3P)AuSec]^+$ along the Au^I-Se bond breaking reaction coordinate by using a step of 0.25 Å for a total of 45 steps (Figure S32, red profile): (on the top) optimized geometries of the first (**uSe-1**) and (on the bottom) the last step (45) of scan calculation. Notably, at the end of the scan calculation Sec remains in its zwitterionic state although the neutral form (SeH, NH_2, COOH) is the lowest energy isomer when considered as an isolated species in the gas-phase. Electron energies relative to the starting geometry (**uSe-1**) are reported in brackets (kJ mol^{-1}).
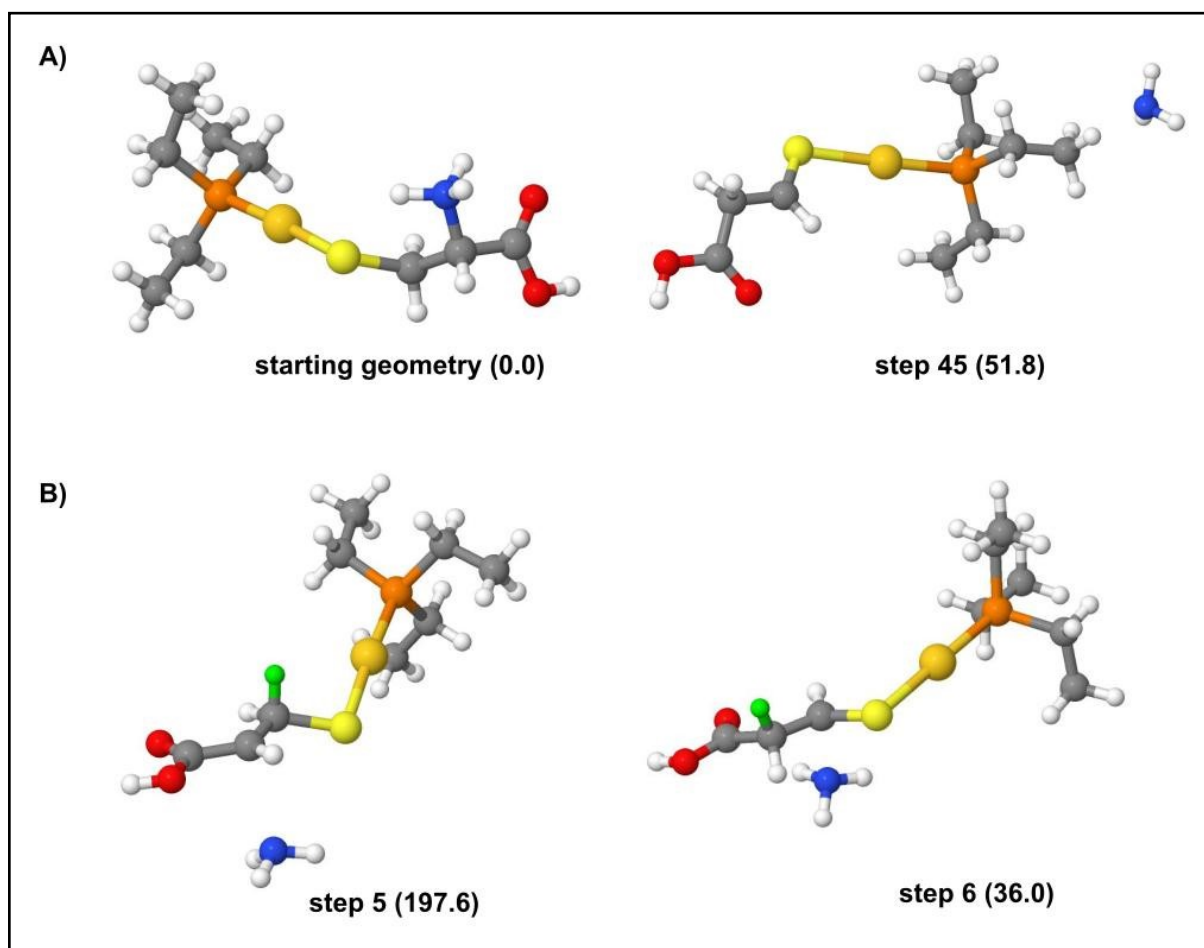
Figure S36: Most relevant optimized geometries of the relaxed scan calculations at the B3LYP/6-311+G(d,p)/LANL2DZ level of theory, computed for $[(Et_3P)AuCys]^+$ along the C_α-NH_3^+ bond breaking reaction coordinate by using a step of 0.25 Å for a total of 45 steps (Figure S33, blue profile): A) optimized geometries of the first (**cS-1**) and the last step (45) of scan calculation; B) optimized structures of highest energy step (step 5) and of the following one (step 6) along the reaction coordinate. The hydride (H) transferred to C_α is colored in green. Electron energies relative to the starting geometry (**cS-1**) are reported in brackets (kJ mol^{-1}).
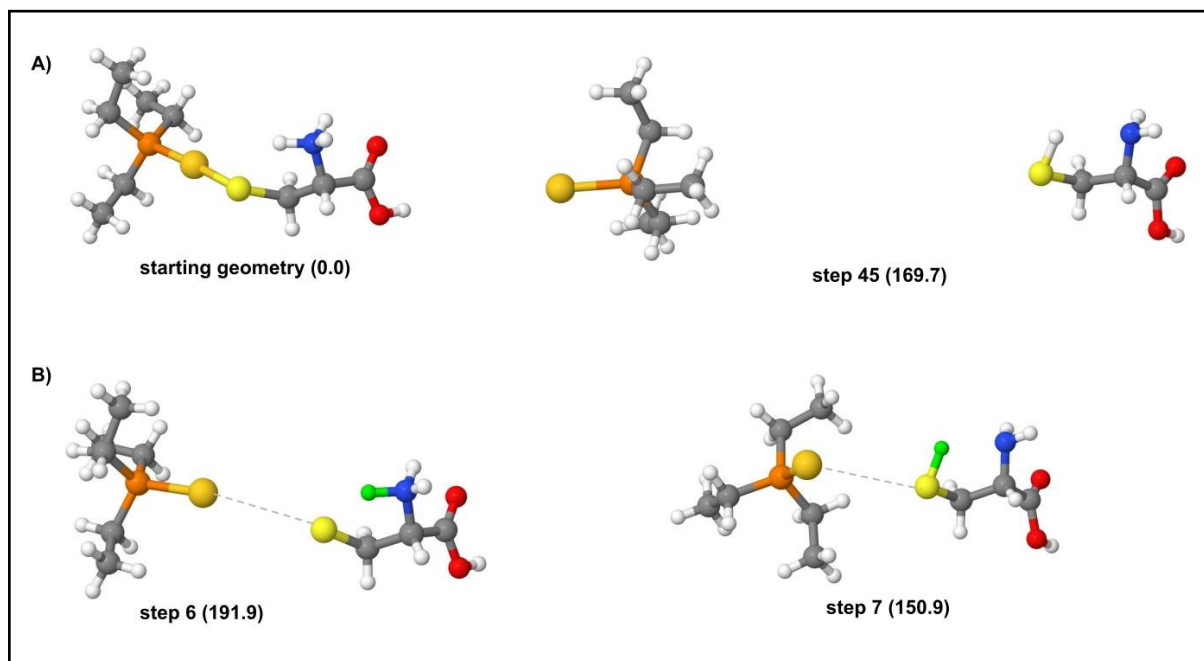
Figure S37: Most relevant optimized geometries of the relaxed scan calculations at the B3LYP/6-311+G(d,p)/LANL2DZ, computed for $[(Et_3P)AuCys]^+$ along the Au^I-S bond breaking reaction coordinate by using a step of 0.25 Å for a total of 45 steps (Figure S34, red profile): A) optimized geometries of the first (**cS-1**) and the last step (45) of scan calculation; B) optimized structures of hypothetical transition state (step 6) and of the subsequent step (step 7) along the reaction coordinate. The H atom transferred to S- from the amino group is colored in green. Electron energies relative to the starting geometry (**cS-1**) are reported in brackets (kJ mol^{-1}).
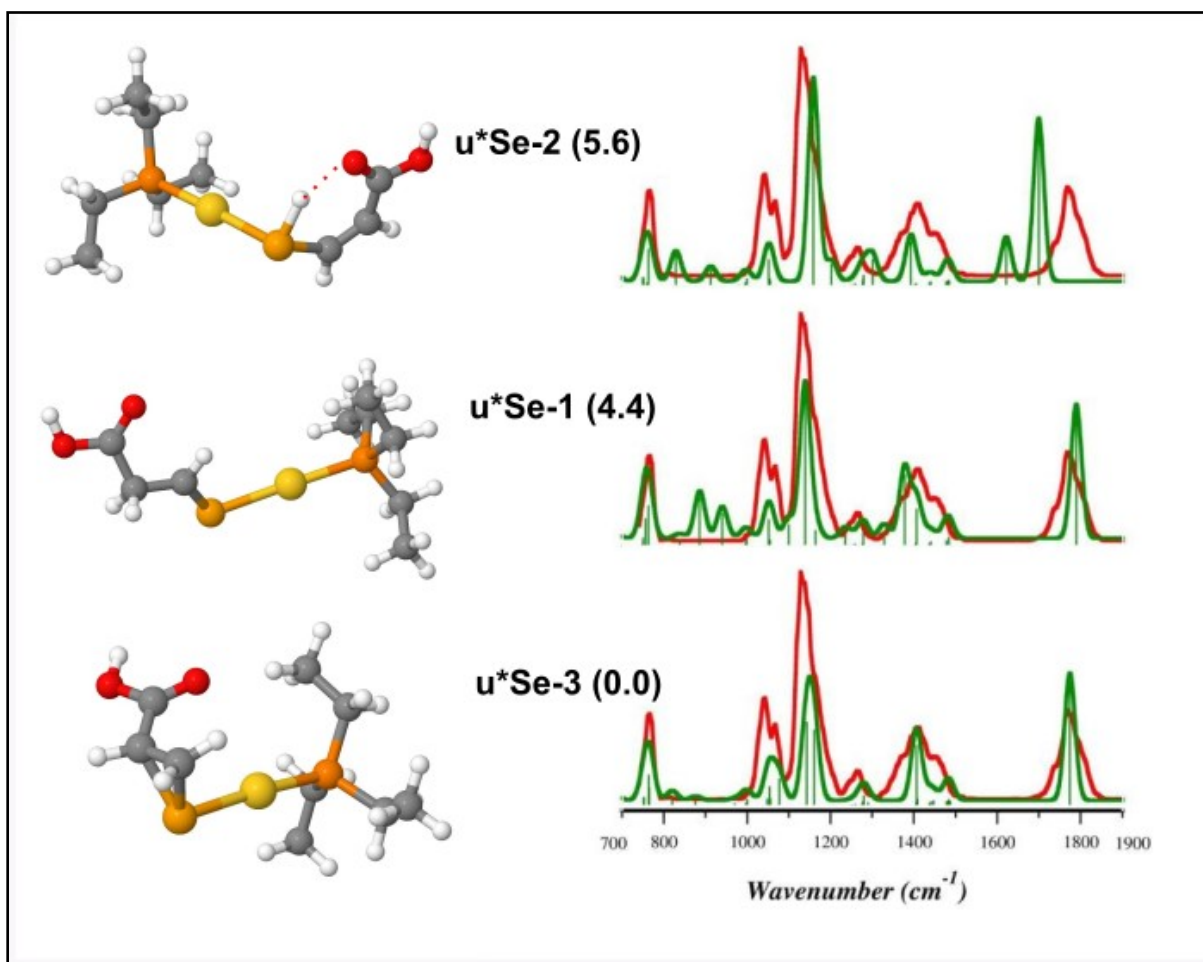
Figure S38: Optimized geometries along with IRMPD spectrum (red profiles) and calculated harmonic IR spectra (green profiles) of the lowest energy isomers of the $[(Et_3P)AuSec^*]^+$ ion, computed in gas phase at B3LYP/BS1 level of theory. Harmonic frequencies computed in the 700−1900 cm^{-1} range were scaled by 0.985. Free energy values relative to **u*Se-3** are reported in parenthesis in kJ mol^{-1}.
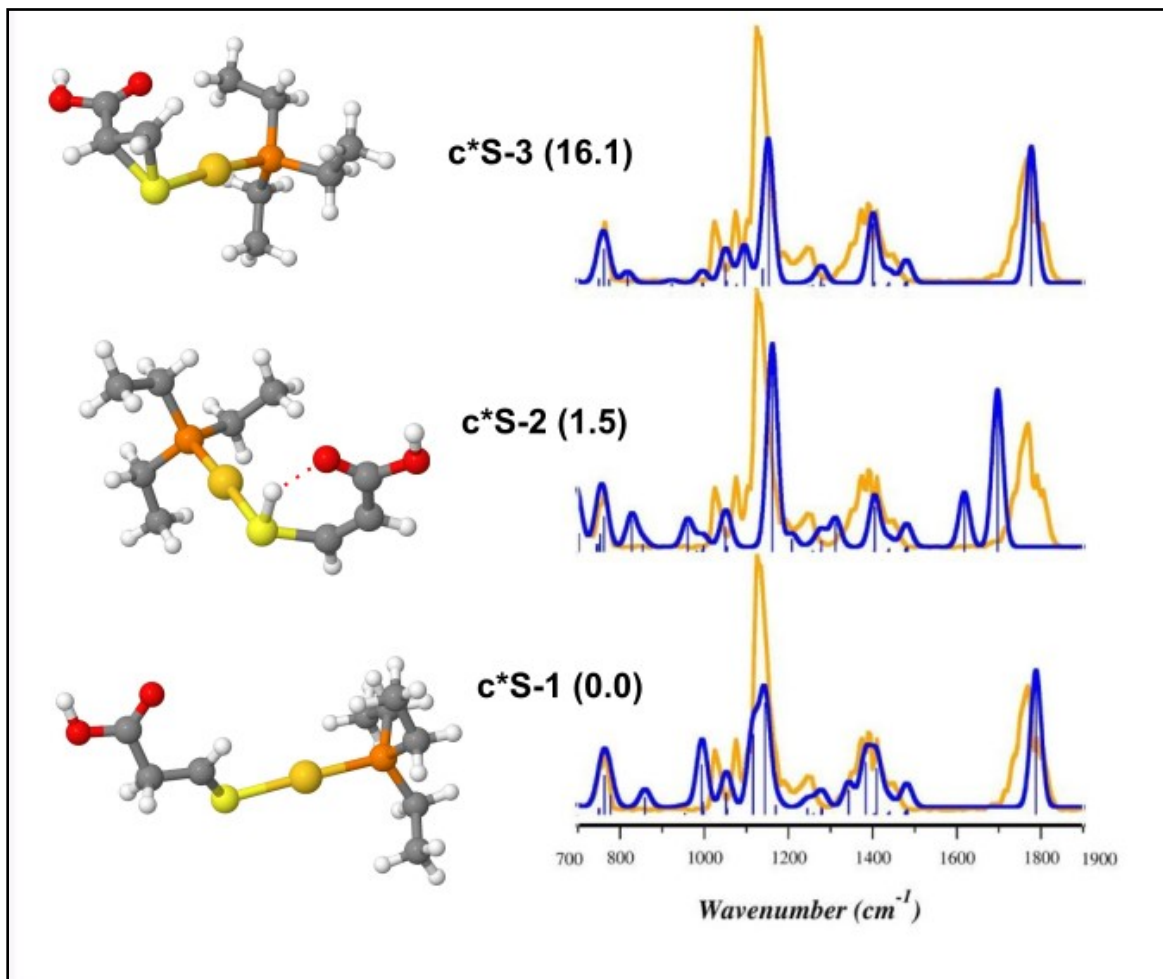
Figure S39: Optimized geometries along with IRMPD spectrum (orange profiles) and calculated harmonic IR spectra (blue profiles) of the lowest energy isomers of the $[(Et_3P)AuCys*]^+$ ion, computed in gas phase at B3LYP/BS1 level of theory. Harmonic frequencies computed in the 700−1900 cm^{-1} range were scaled by 0.985. Free energy values relative to **c*S-1** are reported in parenthesis in kJ mol^{-1}.

Table S1: relative free energies of isomers and conformers of [(Et$_3$P)AuSec]$^+$ ion optimized in the gas phase at the B3LYP/BS1 level of theory.

Isomers/conformers	ΔG (kJ/mol)	Isomers/conformers	ΔG (kJ/mol)
uSe-1	0.0	uN-9	15.1
uSe-2	1.3	uN-10	15.8
uSe-3	2.1	uSeH-1	16.6
uSe-4	2.2	uSeH-2	18.9
uSe-5	4.1	uSeH-3	19.7
uSe-6	4.2	uSeH-4	20.0
uSe-7	4.5	uSeH-5	20.2
uSe-8	4.6	uSeH-6	20.4
uSe-9	4.7	uSeH-7	21.7
uSe-10	5.2	uSeH-8	22.7
uN-1	7.3	uSeH-9	23.0
uN-2	12.0	uSeH-10	23.4
uN-3	13.7	uCOO-1	26.9
uN-4	13.8	uCOO-1	60.5
uN-5	14.0	uCOOH-1	66.9
uN-6	14.1	uCOOH-2	71.3
uN-7	14.8	uCOOH-3	72.1
uN-8	14.9		

Table S2: IRMPD absorptions of $[(Et_3P)AuSec]^+$ ion and calculated vibrational frequencies (cm^{-1}) for **uSe-1**. Calculated intensities are reported in parentheses (km mol^{-1}). Calculated frequencies in the fingerprint (1900-700 cm^{-1}) and X-H stretching (2000-3900 cm^{-1}) ranges are scaled by factors of 0.985 and 0.955, respectively. Modes with intensity lower than 50 km mol^{-1} are omitted.

IRMPD frequencies	Calculated IR frequencies	Assignment
765	771 (65)	ρ CH_2 (Et)
905	906 (52)	v C_α-C_β , δ_{as} N-H
1040	1045 (50)	τ CH_2 (Et)
1090	1108 (69)	δ_{as} N-H, δ C_α-H, δ_s O-H
1150	1165 (321)	δ_s O-H, δ_{as} N-H
-	1340 (54)	δ C_α-H, δ_s O-H
1390	1406 (98)	δ_s O-H, v CO-OH, δ_s NH_2
	1419 (227)	umbrella mode NH_3
1775	1776 (269)	v C=O
2000 - 2800	2669 (1007)	v N-H (involved in H bond with S atom)
2860-2983	2912-2970	v C-H (*low intensity*)
3205	3224 (107)	v N-H (involved in H bond with O=C group)
3350	3343 (103)	v N-H (free)
3540	3554 (174)	v O-H

v: stretching; δ: bending (δ_s: symmetric or scissoring, δ_{as}: antisymmetric); ρ: rocking; τ: twisting.

Table S3: IRMPD absorptions of $[(Et_3P)AuSec]^+$ ion and calculated vibrational frequencies (cm^{-1}) for **uN-1**. Calculated intensities are reported in parentheses (km mol^{-1}). Calculated frequencies in the fingerprint (1900-700 cm^{-1}) and X-H stretching (2000-3900 cm^{-1}) ranges are scaled by factors of 0.985 and 0.955, respectively. Modes with intensity lower than 50 km mol^{-1} are omitted.

IRMPD frequencies	Calculated IR frequencies	Assignment
765	763 (61)	ρ CH$_2$ (Et)
1040	1051 (74)	ρ CH$_2$ (Et)
1090	1060 (82)	v C$_\alpha$-C$_\beta$
1150	1145 (79)	τ NH$_2$, δ_s O-H
	1155 (116)	δ_s O-H, τ NH$_2$
1203 (s)	1222 (85)	ω NH$_2$
	1305 (51)	δ_s O-H, δ C$_\alpha$-H
1390	-	
-	1415 (50)	δ_s NH$_2$
1775	1784 (260)	v C=O
2860-2983	2912-2976	v C-H (*low intensity*)
3205	3197 (149)	v N-H (involved in H bond with SH group)
3350	3284 (94)	v N-H (involved in H bond with O=C group)
3540	3556 (150)	v O-H

v: stretching; δ: bending (δ_s: symmetric or scissoring, δ_{as}: antisymmetric); ρ: rocking; τ: twisting; ω: wagging.

Table S4: IRMPD absorptions of $[(Et_3P)AuSec]^+$ ion and calculated vibrational frequencies (cm^{-1}) for **uSeH-1**. Calculated intensities are reported in parentheses (km mol^{-1}). Calculated frequencies in the fingerprint (1900-700 cm^{-1}) and X-H stretching (2000-3900 cm^{-1}) ranges are scaled by factors of 0.985 and 0.955, respectively. Modes with intensity lower than 50 km mol^{-1} are omitted.

IRMPD frequencies	Calculated IR frequencies	Assignment
765	761 (70)	ρ CH$_2$ (Et)
855	796 (62)	ω NH$_2$, δ_s C$_\beta$H$_2$
1150	1136 (269)	δ_s O-H, τ NH$_2$
1250 - 1290	1303 (50)	δ_s O-H, δ C$_\alpha$-H
-	1634 (57)	δ_s NH$_2$
1775	1780 (291)	v C=O
2000 - 2800	2173 (97)	v S-H
2860-2983	2912-2976	v C-H (*low intensity*)
3205	3357 (22)	v_s NH$_2$
3350	3432 (28)	v_{as} NH$_2$
3540	3574 (89)	v O-H

v: stretching (v_s: symmetric or scissoring, v_{as}: antisymmetric); δ: bending (δ_s: symmetric or scissoring, δ_{as}: antisymmetric); ρ: rocking; τ: twisting; ω: wagging.

Table S5: relative free energies of isomers and conformers of [(Et$_3$P)AuCys]$^+$ ion optimized in the gas phase at the B3LYP/BS1 level of theory.

Isomers/conformers	ΔG (kJ/mol)	Isomers/conformers	ΔG (kJ/mol)
cN-1	0.0	cS-9	12.6
cN-2	0.3	cS-10	13.1
cN-3	0.7	cSH-1	12.4
cN-4	2.3	cSH-2	14.7
cN-5	2.7	cSH-3	15.3
cN-6	3.6	cSH-4	16.4
cN-7	3.9	cSH-5	16.4
cN-8	4.2	cSH-6	16.6
cN-9	4.5	cSH-7	17.5
cN-10	4.5	cSH-8	18.2
cS-1	8.3	cSH-9	18.4
cS-2	8.6	cSH-10	18.5
cS-3	9.1	cCOO-1	17.9
cS-4	10.5	cCOOH-1	42.8
cS-5	11.4	cCOOH-2	55.2
cS-6	11.6	cCOO-2	56.7
cS-7	12.0	cCOOH-3	57.2
cS-8	12.1	cCOOH-4	61.4

Table S6: IRMPD absorptions of $[(Et_3P)AuCys]^+$ ion and calculated vibrational frequencies (cm^{-1}) for **cN-1**. Calculated intensities are reported in parentheses ($km\ mol^{-1}$). Calculated frequencies in the fingerprint (1900-700 cm^{-1}) and X-H stretching (2700-3900 cm^{-1}) ranges are scaled by factors of 0.985 and 0.955, respectively. Modes with intensity lower than 50 $km\ mol^{-1}$ are omitted.

IRMPD frequencies	Calculated IR frequencies	Assignment
773	763 (50)	$\rho\ CH_2$ (Et)
1032	1044 (90)	$\nu\ C_\alpha$-N , $\delta_s\ CH_2$ (Et)
1053	1052 (52)	$\nu\ C_\alpha$-N
1142	1145 (201)	δ_s O-H, $\tau\ NH_2$
	1171 (82)	$\omega\ NH_2$, $\tau\ C_\beta H_2$
-	1213 (70)	$\rho\ NH_2$, $\delta\ C_\alpha$-H
1409	1409 (40)	$\rho\ NH_2$, $\delta\ C_\alpha$-H
1571	1581 (64)	$\delta_s\ NH_2$
1781	1786 (257)	ν C=O
2845 - 3030	2910 - 2978	ν C-H (*low intensity*)
3218	3235 (106)	$\nu_s\ NH_2$
3340	3309 (72)	$\nu_{as}\ NH_2$
3550	3559 (135)	ν O-H

ν: stretching (ν_s: symmetric or scissoring, ν_{as}: antisymmetric); δ: bending (δ_s: symmetric or scissoring, δ_{as}: antisymmetric); ρ: rocking; τ: twisting; ω: wagging.

Table S7: IRMPD absorptions of $[(Et_3P)AuCys]^+$ ion and calculated vibrational frequencies (cm^{-1}) for **cS-1**. Calculated intensities are reported in parentheses (km mol^{-1}). Calculated frequencies in the fingerprint (1900-700 cm^{-1}) and X-H stretching (2700-3900 cm^{-1}) ranges are scaled by factors of 0.985 and 0.955, respectively. Modes with intensity lower than 50 km mol^{-1} are omitted.

IRMPD frequencies	Calculated IR frequencies	Assignment
-	735 (41)	ρ CH$_2$ (Et)
773	765 (42)	ρ CH$_2$ (Et)
-	885 (57)	ν C$_\alpha$-C$_\beta$, δ NH$_3$
-	912 (43)	ν C$_\alpha$-C$_\beta$, δ NH$_3$
1053, 1032	1045 (64)	δ CH$_2$ (Et)
1142	1110 (88)	ω NH$_2$, δ C$_\alpha$-H
	1165 (313)	δ_s O-H
-	1337 (60)	δ C$_\alpha$-H, δ_s O-H
1409	1404 (198)	umbrella mode NH$_3$, δ C$_\alpha$-H
	1412 (177)	umbrella mode NH$_3$, δ_s O-H
1781	1776 (273)	ν C=O
-	2649 (1018)	ν_{as} NH$_3$ (N-H … S)
2845 - 3030	2903 - 2977	ν C-H (*low intensity*)
3218	3225 (113)	ν_{as} NH$_3$ (N-H … O=C)
3340	3347 (105)	ν_{as} NH$_3$
3550	3554 (171)	ν O-H

ν: stretching (ν_s: symmetric or scissoring, ν_{as}: antisymmetric); δ: bending (δ_s: symmetric or scissoring, δ_{as}: antisymmetric); ρ: rocking; τ: twisting; ω: wagging.
Vibrational mode with intensity below 50

Table S8: IRMPD absorptions of [(Et$_3$P)AuCys]$^+$ ion and calculated vibrational frequencies (cm^{-1}) for **cSH-1**. Calculated intensities are reported in parentheses (km mol^{-1}). Calculated frequencies in the fingerprint (1900-700 cm^{-1}) and X-H stretching (2700-3900 cm^{-1}) ranges are scaled by factors of 0.985 and 0.955, respectively. Modes with intensity lower than 50 km mol^{-1} are omitted.

IRMPD frequencies	Calculated IR frequencies	Assignment
-	721 (52)	δ Cys (molecular deformation)
773	769 (65)	ρ CH$_2$ (Et)
-	821 (68)	δ SH, ω NH$_2$
1032, 1053	-	
1142	1137 (271)	δ_s O-H
1409	-	
1571	1635 (56)	δ_s NH$_2$
1781	1780 (298)	v C=O
-	2421 (177)	v S-H
2845 - 3030	2984 - 2897	v C-H (*low intensity*)
3218	3359 (22)	v_s NH$_2$
3340	3433 (30)	v_{as} NH$_2$
3550	3572 (94)	v O-H

v: stretching (v_s: symmetric or scissoring, v_{as}: antisymmetric); δ: bending (δ_s: symmetric or scissoring, δ_{as}: antisymmetric); ρ: rocking; τ: twisting; ω: wagging.
Vibrational mode with intensity below 50

Table S9: relative free energies of isomers and conformers of deaminated $[(Et_3P)AuSec^*]^+$ and $[(Et_3P)AuCys^*]^+$ ions optimized in the gas phase at the B3LYP/BS1 level of theory.

Isomers/conformers	ΔG (kJ/mol)	Isomers/conformers	ΔG (kJ/mol)
u*Se-3	0.0	c*S-1	0.0
u*Se-1	4.4	c*S-2	1.5
u*Se-2	5.6	c*S-3	16.1

Table S10: IRMPD absorptions of $[(Et_3P)AuSec^*]^+$ ion and calculated vibrational frequencies (cm^{-1}) for **u*Se-3**. Calculated intensities are reported in parentheses ($km\ mol^{-1}$). Calculated frequencies in the fingerprint (1900-700 cm^{-1}) and range are scaled by factors of 0.985. Non relevant modes with intensity lower than 50 $km\ mol^{-1}$ are omitted.

IRMPD frequencies	Calculated IR frequencies	Assignment
769	762 (59)	$\delta\ CH_2/CH_3$ (Et)
1045	1053 (36)	$\tau\ CH_2/CH_3$ (Et)
1071	1076 (51)	$\delta\ C_\alpha$-H, $\omega\ C_\beta H_2$
1133	1142 (160)	ν C-OH, $\nu\ C_\alpha$-C_β
	1159 (145)	$\nu\ C_\alpha$-C_β, $\delta\ C_\beta H_2$
1273	1279 (19)	$\delta\ CH_2/CH_3$ (Et)
1418	1406 (116)	δ_s O-H, $\nu\ C_\alpha$-COOH
1777	1773 (244)	ν C=O

ν: stretching (ν_s: symmetric or scissoring, ν_{as}: antisymmetric); δ: bending (δ_s: symmetric or scissoring, δ_{as}: antisymmetric); ρ: rocking; τ: twisting; ω: wagging.

Table S11: IRMPD absorptions of $[(Et_3P)AuSec*]^+$ ion and calculated vibrational frequencies (cm^{-1}) for **u*Se-1**. Calculated intensities are reported in parentheses ($km\ mol^{-1}$). Calculated frequencies in the fingerprint (1900-700 cm^{-1}) and range are scaled by factors of 0.985. Non relevant modes with intensity lower than 50 $km\ mol^{-1}$ are omitted.

IRMPD frequencies	Calculated IR frequencies	Assignment
769	755 (51)	δ C$_\beta$-H
	762 (76)	δ CH$_2$/CH$_3$ (Et)
-	886 (91)	δ C$_\beta$-H,
-	939 (61)	ρ C$_\alpha$H$_2$, δ C$_\beta$-H
1045	1050 (50)	δ CH$_2$/CH$_3$ (Et)
1071	1098 (40)	v C$_\alpha$-C$_\beta$
1133	1138 (298)	v C-OH, δ_s O-H, δ C$_\alpha$H$_2$, δ C$_\beta$H
1273	1277 (29)	δ CH$_2$/CH$_3$ (Et)
1418	1377 (136)	δ_s O-H, v C$_\alpha$-COOH
	1406 (70)	δ_s C$_\alpha$H$_2$
1777	1789 (258)	v C=O

v: stretching (v_s: symmetric or scissoring, v_{as}: antisymmetric); δ: bending (δ_s: symmetric or scissoring, δ_{as}: antisymmetric); ρ: rocking; τ: twisting; ω: wagging.

Table S12: IRMPD absorptions of $[(Et_3P)AuCys*]^+$ ion and calculated vibrational frequencies (cm^{-1}) for **c*S-1**. Calculated intensities are reported in parentheses ($km\ mol^{-1}$). Calculated frequencies in the fingerprint (1900-700 cm^{-1}) and range are scaled by factors of 0.985. Non relevant modes with intensity lower than 50 $km\ mol^{-1}$ are omitted.

IRMPD frequencies	Calculated IR frequencies	Assignment
769	762 (75)	$\delta\ CH_2/CH_3$ (Et)
1028	994 (96)	$\delta\ CH_2/CH_3$ (Et), cys deformation
1084	1052 (43)	$\tau\ CH_2/CH_3$ (Et)
1128	1116 (154)	$v\ C_\alpha$-C_β, δ_s O-H
1145	1144 (214)	v C-OH, δ_s O-H, $\delta\ C_\beta H$
1255	-	
	1344 (47)	$\delta\ C_\beta H$, δ_s O-H
1396 (1373 - 1418)	1383 (101)	δ_s O-H, $\delta_s\ C_\alpha H_2$
	1410 (89)	$\delta_s\ C_\alpha H_2$
1772	1788 (260)	v C=O

v: stretching (v_s: symmetric or scissoring, v_{as}: antisymmetric); δ: bending (δ_s: symmetric or scissoring, δ_{as}: antisymmetric); ρ: rocking; τ: twisting; ω: wagging.

Table S13: IRMPD absorptions of $[(Et_3P)AuCys^*]^+$ ion and calculated vibrational frequencies (cm^{-1}) for **c*S-3**. Calculated intensities are reported in parentheses $(km\ mol^{-1})$. Calculated frequencies in the fingerprint $(1900-700\ cm^{-1})$ and range are scaled by factors of 0.985. Non relevant modes with intensity lower than $50\ km\ mol^{-1}$ are omitted.

IRMPD frequencies	Calculated IR frequencies	Assignment
769	763 (71)	δ CH$_2$/CH$_3$ (Et)
1028	1051 (45)	δ CH$_2$/CH$_3$ (Et)
1084	1097 (70)	δ C$_\alpha$-H
1128	-	
1145	1153 (256)	v C-OH, δ_s O-H
1255	-	
1396 (1373 - 1418)	1402 (120)	δ_s O-H, δ C$_\alpha$-H, δ C$_\beta$H$_2$
1772	1778 (259)	v C=O

v: stretching (v_s: symmetric or scissoring, v_{as}: antisymmetric); δ: bending (δ_s: symmetric or scissoring, δ_{as}: antisymmetric); ρ: rocking; τ: twisting; ω: wagging.